

Small-RNA-mediated transgenerational silencing of histone genes impairs fertility in piRNA mutants

Giorgia Barucci^{1,2,7}, Eric Cornes^{1,7}, Meetali Singh^{1,7}, Blaise Li³, Martino Ugolini^{1,4}, Aleksei Samolygo^{1,5}, Celine Didier¹, Florent Dingli^{1,6}, Damarys Loew^{1,6}, Piergiuseppe Quarato^{1,2} and Germano Cecere^{1*}

PIWI-interacting RNAs (piRNAs) promote fertility in many animals. However, whether this is due to their conserved role in repressing repetitive elements (REs) remains unclear. Here, we show that the progressive loss of fertility in *Caenorhabditis elegans* lacking piRNAs is not caused by derepression of REs or other piRNA targets but, rather, is mediated by epigenetic silencing of all of the replicative histone genes. In the absence of piRNAs, downstream components of the piRNA pathway relocalize from germ granules and piRNA targets to histone mRNAs to synthesize antisense small RNAs (sRNAs) and induce transgenerational silencing. Removal of the downstream components of the piRNA pathway restores histone mRNA expression and fertility in piRNA mutants, and the inheritance of histone sRNAs in wild-type worms adversely affects their fertility for multiple generations. We conclude that sRNA-mediated silencing of histone genes impairs the fertility of piRNA mutants and may serve to maintain piRNAs across evolution.

Among the different classes of endogenous sRNAs in animals, PIWI-interacting RNAs (piRNAs) play a conserved role in repressing transposons and other repetitive elements (REs)¹; in several animal species, the loss of piRNAs causes sterility². Owing to the role of piRNAs in transposon silencing, the sterility phenotype observed in animals lacking piRNAs is commonly thought to be caused by derepression of REs and, consequently, DNA damage³. However, non-transposon-derived piRNAs promote fertility in mice⁴, and a piRNA-independent function of one of the PIWI proteins, MIWI, has been implicated in male fertility⁵. The requirement of piRNAs and PIWI for animal fertility can therefore be uncoupled from their role in transposon silencing and might be due to additional piRNA regulatory functions. In *C. elegans*, mutations in components of the piRNA pathway show progressive loss of fertility across generations, ultimately leading to a sterile population of worms⁶. This transgenerational phenotype is often temperature dependent and reversible; animals of this phenotype gradually become sterile at increased temperature and recover their fertility when grown at a lower temperature^{7–10}. Thus, whether the role of piRNAs in promoting fertility depends on silencing REs or other epigenetic mechanisms remains a matter of debate¹¹.

The majority of *C. elegans* piRNAs are independently transcribed in the germline from thousands of genomic loci and do not have sequence complementarity to REs^{12–16}. However, these piRNAs regulate their targets by imperfect complementarity^{17,18}. Thus, any REs or other germline-expressed RNA sequences, including protein-coding transcripts, are potential targets and their regulation can also contribute to promoting fertility. *C. elegans* piRNAs do not directly silence the expression of their targets, but trigger the accumulation of small single-stranded antisense 22G-RNAs, which are loaded into

worm-specific argonaute proteins (WAGOs). These constitute the downstream effector factors of the piRNA-induced silencing pathway and silence the complementary targets at the transcriptional and the post-transcriptional levels^{8,19,20}. PIWI and its downstream effectors localize to specific perinuclear compartments called germ granules, and some of the structural components of germ granules also participate in heritable RNA interference (RNAi)^{21–23}.

Here, we investigate the mechanisms that underlie the transgenerational loss of fertility in a population of *C. elegans* that lacks piRNAs. We show that the removal of piRNAs is not sufficient to derepress protein coding and RE transcripts targeted by the piRNA pathway. Instead, we found that, in the absence of piRNAs, the downstream effectors of piRNA-induced silencing complex relocalize from piRNA targets to histone mRNAs. This process leads to the accumulation of 22G-RNAs antisense to all of the replicative histone genes and to the transgenerational silencing of histone mRNAs, ultimately leading to sterile animals.

Results

piRNA targets are not desilenced in *piwi*-mutant worms. To understand the reduced fertility and transgenerational sterility observed in piRNA mutants^{5,12,14}, we identified transcripts that are directly regulated by piRNAs. We combined sRNA sequencing (sRNA-seq) with strand-specific RNA-seq and compared *C. elegans* with a mutation in the PIWI protein PRG-1 with wild-type worms, using populations of synchronized young adult worms carrying the null allele *prg-1(n4357)*¹⁴, which are almost sterile at 20 °C (Extended Data Fig. 1a). To identify piRNA-dependent 22G-RNA protein-coding targets, we selected 1,017 protein-coding genes from which substantially reduced levels of

¹Mechanisms of Epigenetic Inheritance, Department of Developmental and Stem Cell Biology, Institut Pasteur, UMR 3738, CNRS, Paris, France. ²Sorbonne Université, Collège doctoral, Paris, France. ³Bioinformatics and Biostatistics Hub, C3BI, Institut Pasteur, USR 3756, CNRS, Paris, France. ⁴Scuola Normale Superiore, Pisa, Italy. ⁵Moscow Institute of Physics and Technology, Moscow, Russia. ⁶Centre de Recherche, Laboratoire de Spectrométrie de Masse Protéomique, Institut Curie, PSL Research University, Paris, France. ⁷These authors contributed equally: Giorgia Barucci, Eric Cornes, Meetali Singh.

*e-mail: germano.cecere@pasteur.fr

22G-RNAs were produced (less than fourfold) in the *prg-1(n4357)* mutant compared with wild-type worms. Only 6% (67 genes) of these mRNA transcripts became upregulated (more than twofold; adjusted $P < 0.05$; Fig. 1a). Analysis of 958 RE families revealed that 154 REs had reduced levels of 22G-RNAs (less than twofold) in *prg-1(n4357)* compared with wild-type worms, yet only three families of REs were significantly upregulated (more than twofold; adjusted $P < 0.05$; Fig. 1b). We also used uniquely mapped reads to analyse the expression of approximately 60,000 discrete REs²⁴ and found that less than 100 individual REs were significantly upregulated (by at least twofold; adjusted $P < 0.05$) in *piwi*-mutant compared with wild-type worms (Extended Data Fig. 1b,d). The decrease in 22G-RNAs antisense to protein-coding genes or REs was therefore not sufficient to derepress these genes, and they were probably kept repressed by nuclear RNAi and/or chromatin factors^{24–26}. Indeed, RNA-seq analysis and quantitative PCR with reverse transcription (RT-qPCR) of individual REs in the mutant of the nuclear argonaute HRDE-1—a downstream effector of the piRNA pathway that acts at the transcriptional level—resulted in a larger number of upregulated REs compared with the *prg-1(n4357)* mutant (Extended Data Fig. 1b,d). Nonetheless, the *hrde-1(tm1200)* mutant that we analysed was not sterile and showed only a mild reduction in fertility compared with wild-type worms (Extended Data Fig. 1a), suggesting that the derepression of REs might not be correlated with the piRNA-mutant phenotype. These results also suggest that piRNAs might be required to only initiate, and not to maintain, the silencing of their targets as proposed by previous research^{19,27–29}.

Histone mRNA silencing correlates with transgenerational sterility in *piwi*-mutant worms. The RNA-seq and sRNA-seq analyses also revealed that several protein-coding genes showed a reduction in mRNA levels and increased levels of 22G-RNAs in *prg-1(n4357)* compared with wild-type worms (Fig. 1a), suggesting that they had been silenced by sRNAs. The majority of these transcripts corresponded with the replicative histone mRNAs (Fig. 1a), and most of the histone gene clusters acquired a substantial number of 22G-RNAs, causing substantial downregulation in their complementary mRNAs (Fig. 1c). Using RT-qPCR, we also analysed mRNA levels in worms carrying a mutation in the piRNA biogenesis factor PRDE-1 (ref. ³⁰), and observed a substantial depletion of histone mRNAs (Extended Data Fig. 1c). Mutations in the nuclear argonaute HRDE-1 did not silence histone mRNAs (Extended Data Fig. 1c,e), and nascent RNA-seq (nRNA-seq) revealed only a mild downregulation of some histone genes in *prg-1(n4357)* worms compared with the wild type (Extended Data Fig. 1f,g), indicating that the downregulation of the histone genes occurred at the post-transcriptional level in piRNA mutants.

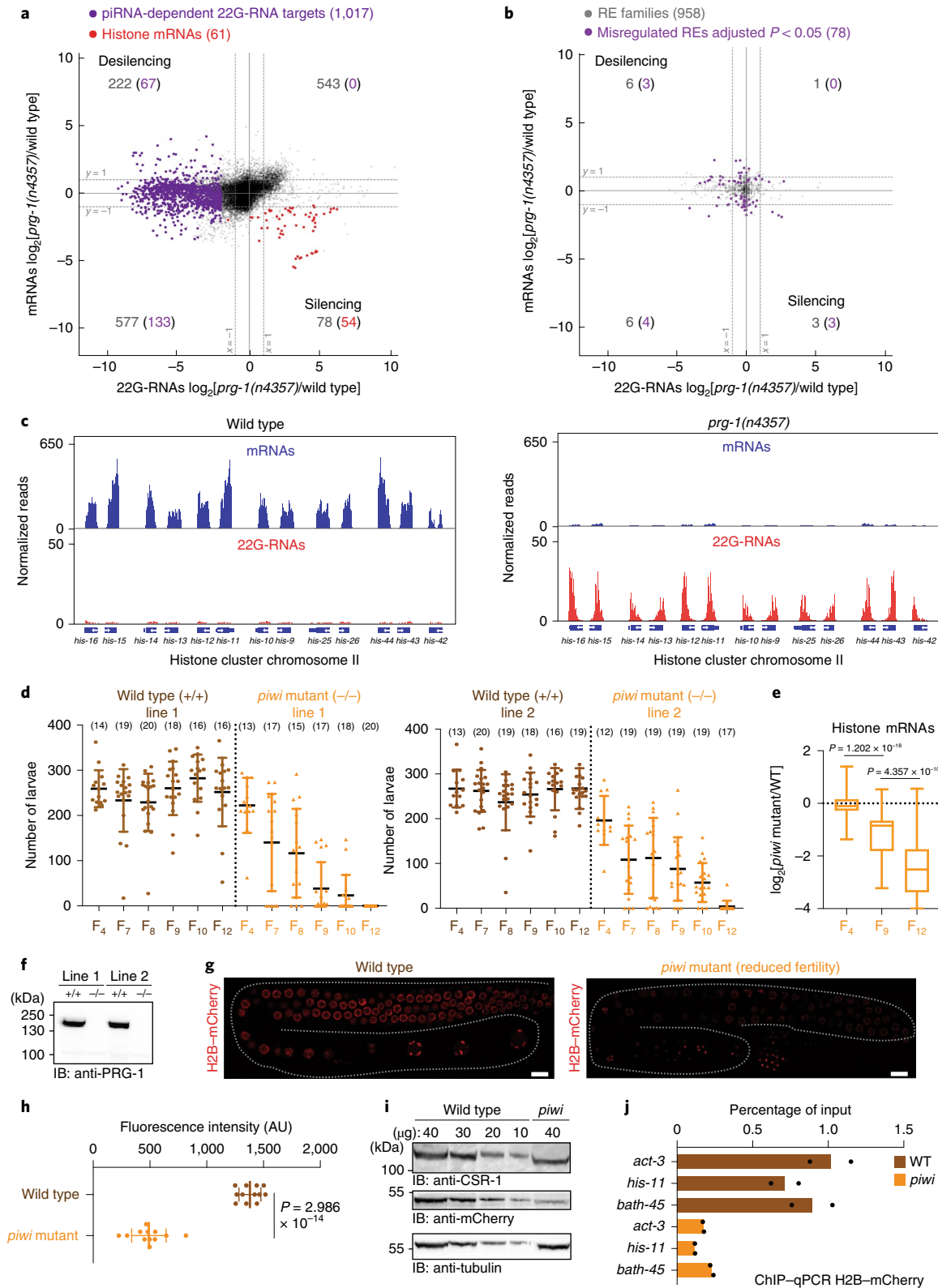
In *C. elegans*, histone mRNA silencing using RNA interference (RNAi) is sufficient to cause sterility^{31,32}. We therefore tested whether histone mRNA silencing correlated with piRNA mutant transgenerational loss of fertility. We generated a CRISPR-Cas9 null allele of the PIWI protein PRG-1, selected two independently edited CRISPR-Cas9 lines and propagated isogenic populations of homozygote *piwi*-mutant and wild-type worms (Fig. 1f). We maintained these lines for ten generations until the *piwi* mutant became almost completely sterile (Fig. 1d), sampling the populations using RNA-seq and sRNA-seq. Mutant worms that were propagated for two generations after homozygosis (F_4) showed no phenotypic differences compared to the wild-type worms (Fig. 1d), and RNA-seq analysis showed that there were very few gene expression changes (Extended Data Fig. 2a). At later generations, individuals from the *piwi*-mutant isogenic population started to display defects in fertility, including full sterility in some individuals, until the population became almost completely sterile after ten generations (Fig. 1d). These results correlated with substantial changes in gene expression across generations (Extended Data Fig. 2a–c). The progressive loss of fertility was accompanied by a gradual reduction of histone mRNA transcripts and a gain of 22G-RNAs antisense to histone mRNAs (Fig. 1e, Extended Data Fig. 2d). The modest desilencing of piRNA-dependent 22G-RNA protein-coding and RE targets did not correlate with the progressive loss of fertility (Extended Data Fig. 2d–f). To evaluate the impact of histone-mRNA silencing on histone protein levels in germ cells, we generated a CRISPR-Cas9 null allele of PIWI in a transgenic strain expressing a single-copy of histone H2B::mCherry in the germline. Live imaging of wild-type worms confirmed that the H2B-mCherry was normally expressed in the germline and incorporated into chromosomes (Fig. 1g, Extended Data Fig. 2h). However, *piwi* mutants showed significantly reduced levels of H2B-mCherry in germline nuclei of animals with reduced fertility (Fig. 1g, h, Extended Data Fig. 2g). Western blotting analysis confirmed the reduced levels of H2B-mCherry in populations of *piwi* mutant worms (Fig. 1i), and chromatin immunoprecipitation (ChIP) experiments revealed a reduction in incorporation of H2B-mCherry into the chromatin of *piwi*-mutant animals (Fig. 1j). These results are in accordance with the observed defect in chromosome compaction in pachytene nuclei of sterile *piwi*-mutant animals (Extended Data Fig. 2h), which can be a consequence of a lack of histone incorporation into chromatin. Together, these results suggest that the transgenerational silencing of histone mRNAs, and not the desilencing of piRNA targets, correlates with the progressive loss of fertility observed in *piwi*-mutant worms.

The downstream component of the PIWI pathway, WAGO-1, targets histone mRNAs for silencing. To identify RNAi factors that are involved in histone mRNA silencing, we investigated

Fig. 1 | Silencing of histone mRNA correlates with progressive sterility in *piwi*-mutant worms. **a**, Comparison between log₂-transformed fold changes in mRNA and 22G-RNA in *prg-1(n4357)* mutant versus wild-type worms for protein-coding genes. The dashed lines indicate twofold changes and the numbers in parentheses indicate the portion of misregulated piRNA-dependent 22G-RNA targets (purple) or histone genes (red) (two-fold changes; adjusted $P < 0.05$, Wald test). The average from two biologically independent replicates is shown. **b**, A similar comparison as shown in **a** for misregulated RE families (adjusted $P < 0.05$, Wald test). The average from two biologically independent replicates is shown. **c**, Genomic view of one histone gene cluster showing mRNAs (blue) and 22G-RNAs (red) in wild-type (left) and *prg-1(n4357)* mutant (right) lines. **d**, Brood size of the two CRISPR-Cas9 *piwi*-mutant (–/–) and wild-type (+/+) lines. The data points correspond to the number of living larvae from individual worms. Data are mean \pm s.d. The sample size n (worms) is indicated in parentheses. **e**, log₂-transformed fold change of histone mRNA in CRISPR-Cas9 *piwi*-mutant worms compared with wild-type worms across generations. The line indicates the median, the box indicates the first and third quartiles, and the whiskers indicate the highest and lowest value. Two-tailed P values were calculated using Mann-Whitney–Wilcoxon tests; $n = 61$ genes. **f**, Immunoblot (IB) showing PIWI protein in the wild-type and *piwi*-mutant lines. The experiment was repeated twice. **g,h**, Representative images (**g**) and quantification (**h**) of germline-expressed H2B-mCherry in wild-type and *piwi*-mutant worms. Scale bars, 10 μ m. Data are mean intensity \pm s.d. from 15 pachytene nuclei in each worm. Statistical analysis was performed using two-tailed unpaired t -tests; $n = 12$ worms. **i**, Immunoblot showing H2B-mCherry in wild-type and *piwi*-mutant worms. Ubiquitous (tubulin) and germline (CSR-1) proteins are shown as control. The experiment was repeated twice. **j**, H2B::mCherry ChIP-qPCR in wild-type and *piwi*-mutant worms. The amount of immunoprecipitated DNA is shown as percentage of input. The bars indicate the mean and the black dots individual data from two biologically independent experiments. Source data are available online.

whether argonaute proteins downstream of PIWI in the piRNA-induced silencing pathway ectopically load sRNAs derived from histone mRNA transcripts. We identified several argonaute proteins that interact with PIWI using mass spectrometry (MS), among which many are known to participate in piRNA-induced silencing²⁰ (Fig. 2a, Supplementary Table 1a). The most highly

enriched PIWI-interacting argonaute protein was WAGO-1, which has a role in the post-transcriptional silencing of piRNA targets^{19,33}. We generated a Flag-tagged version of WAGO-1 and confirmed the interaction between WAGO-1 and PIWI using MS and co-immunoprecipitation (co-IP) experiments (Fig. 2c, Extended Data Fig. 4a). We next immunoprecipitated WAGO-1-associated



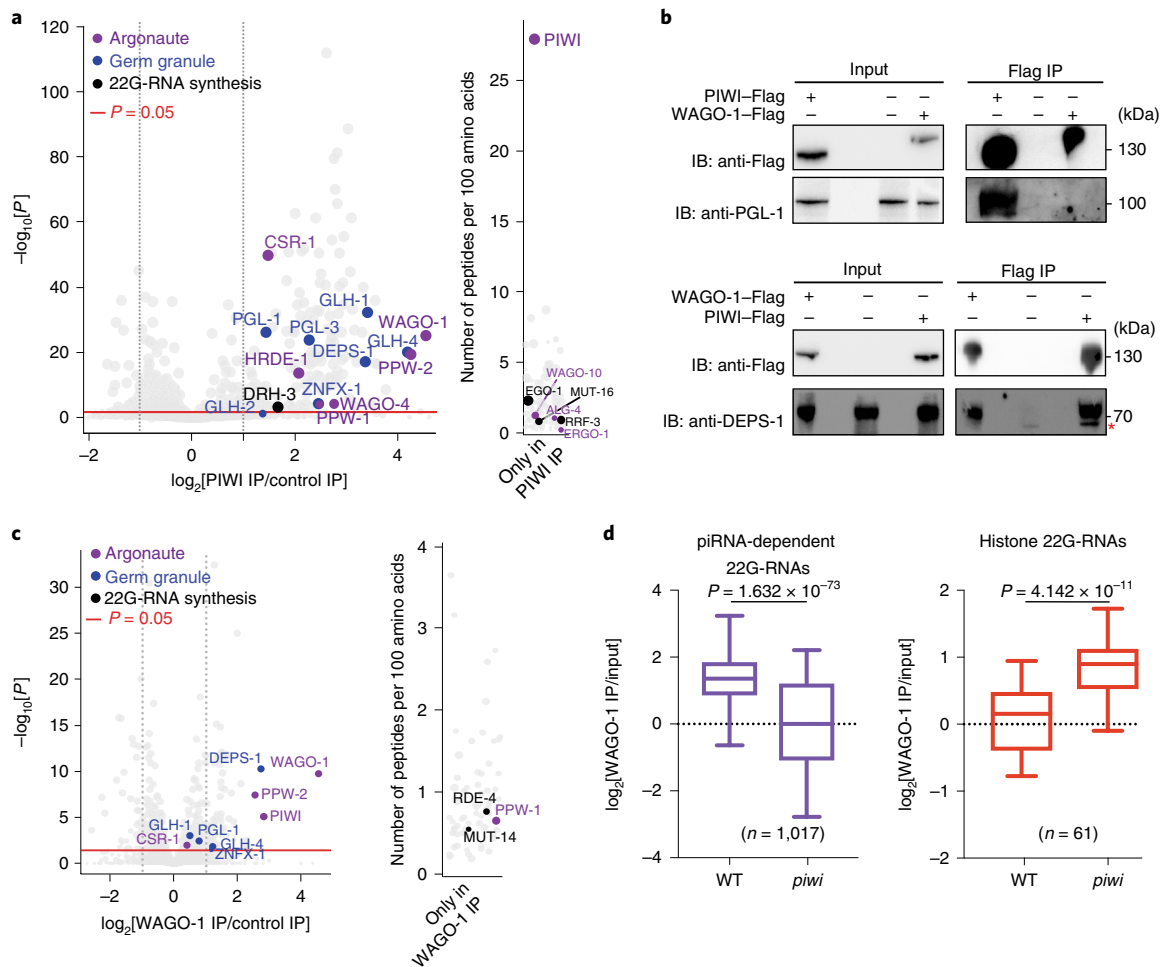


Fig. 2 | Loading histone 22G-RNAs into WAGO-1 after disruption of the piRNA-induced silencing complex. **a**, Enrichment values and corresponding significance levels for proteins that co-purified with PIWI (Supplementary Table 1a). Argonaute proteins, germ-granule components and 22G-RNA biogenesis factors are labelled with different colours. The size of the dots is proportional to the number of peptides used for the quantification. The linear model was used to compute the protein quantification ratio and the red horizontal line indicates two-tailed $P = 0.05$; $n = 4$ biologically independent experiments. **b**, Co-IP experiments showing DEPS-1 interactions between PIWI and WAGO-1, as well as interaction between PGL-1 and PIWI, but not with WAGO-1. The presence (+) or absence (–) of the tagged proteins is indicated. IP was performed using anti-Flag antibodies, and the blots were probed with anti-PGL-1, anti-DEPS-1 or anti-Flag antibodies. The red asterisk indicates that the lower band signal corresponds to a non-specific protein. The experiment was repeated twice. **c**, The \log_2 -transformed fold change and corresponding significance levels of proteins that co-purified with WAGO-1 in wild-type worm lysate as in **a** (Supplementary Table 1b). Argonaute proteins, germ-granule components and 22G-RNA biogenesis factors are labelled with different colours. The size of the dots is proportional to the number of peptides used for quantification. The linear model was used to compute protein quantification ratio and the red horizontal line indicates two-tailed $P = 0.05$; $n = 4$ biologically independent experiments. **d**, The \log_2 -transformed fold change of the ratio between piRNA-dependent 22G-RNA and histone-22G-RNA-normalized reads from WAGO-1 IP and total RNA (input) in wild-type and *piwi* mutant backgrounds. The line indicates the median value, the box indicates the first and third quartiles, and the whiskers indicate the 5th and 95th percentiles. Statistical analysis was performed using two-tailed Mann-Whitney-Wilcoxon tests; $n = 1,017$ genes for piRNA-dependent targets and $n = 61$ genes for histone genes. Source data are available online.

22G-RNAs in wild-type and *piwi*-mutant backgrounds. In the wild-type background, WAGO-1 was loaded with 22G-RNAs derived from piRNA-dependent protein-coding targets (Fig. 2d), and was not enriched in 22G-RNAs from histone mRNAs (Fig. 2d). In the *piwi*-mutant worms, WAGO-1 was instead enriched in histone 22G-RNAs, and the loading of 22G-RNAs derived from piRNA-dependent 22G-RNA targets was significantly decreased (Fig. 2d). Furthermore, in *piwi*-mutant worms, WAGO-1 decreases its interaction with mRNAs from piRNA-dependent 22G-RNA targets and instead binds to histone mRNAs (Extended Data Fig. 3a). These results indicate that WAGO-1 relocated from piRNA-dependent targets to histone mRNAs in a 22G-RNA-dependent manner, suggesting that WAGO-1 is one

of the argonaute proteins that promotes histone mRNA silencing in piRNA-mutant worms.

WAGO-1 gradually loses interaction with germ-granule components after *piwi* mutation. The quantification of PIWI-interacting proteins using MS revealed, in addition to enrichment of argonaute proteins and 22G-RNA biogenesis factors, enrichment of specific germ-granule components, which are also known to participate in heritable RNAi^{21–23} (Fig. 2a–c, Supplementary Table 1a). WAGO-1 also interacts with some germ-granule factors, and preferentially with DEPS-1 (Fig. 2b,c, Extended Fig. 4a, Supplementary Table 1b), which is a germ-granule component that is known to participate in RNAi³⁴. Many of these factors act downstream of the piRNAs to

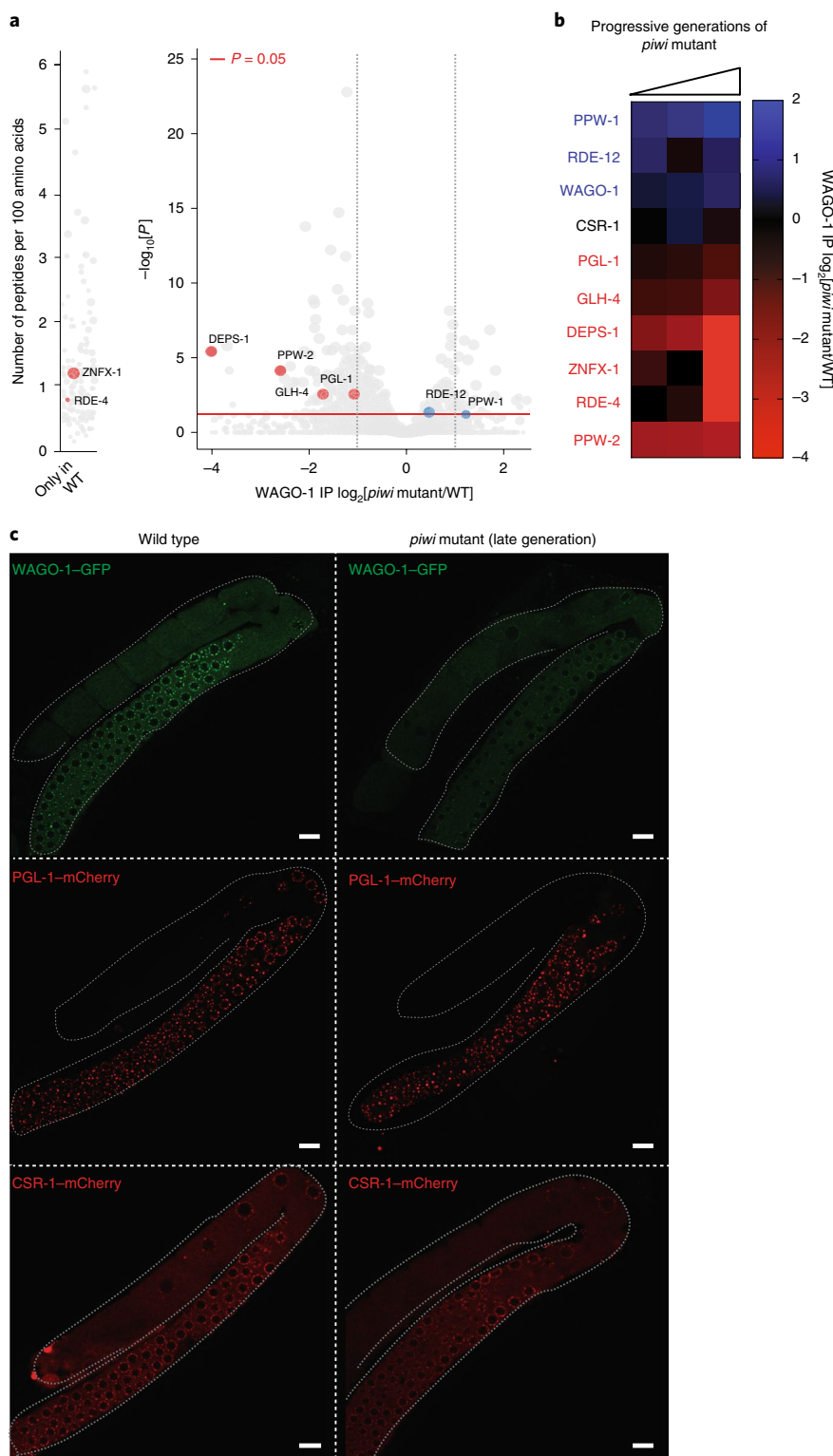


Fig. 3 | WAGO-1 loses interactions with germ-granule components across generations of *piwi*-mutant worms and remains cytoplasmic. **a**, The \log_2 -transformed fold change and corresponding significance levels of proteins co-purifying with WAGO-1 in *piwi*-mutant compared with wild-type lines. Significantly decreased or increased interactions with WAGO-1-interacting germ-granule components, argonaute proteins or RNAi factors are shown in red and blue, respectively. The size of the dots is proportional to the number of peptides that were used for quantification. The linear model was used to compute protein quantification ratio and the red horizontal line indicates two-tailed $P=0.05$; $n=4$ biologically independent experiments. **b**, Heat map of the \log_2 -transformed fold change of proteins co-purifying with WAGO-1 in *piwi*-mutant worms at different generations compared with wild-type worms. Decreased or increased interactions with WAGO-1-interacting germ-granule components, argonaute proteins or RNAi factor are shown in red and blue, respectively; $n=4$ biologically independent experiments. **c**, Live confocal images of WAGO-1-GFP, PGL-1-mCherry and CSR-1-mCherry showing the loss of WAGO-1 germ-granule localization in affected *piwi*-mutant germlines compared with the wild type. Scale bars, 10 μm . The experiment was repeated independently three times with similar results. Source data are available online.

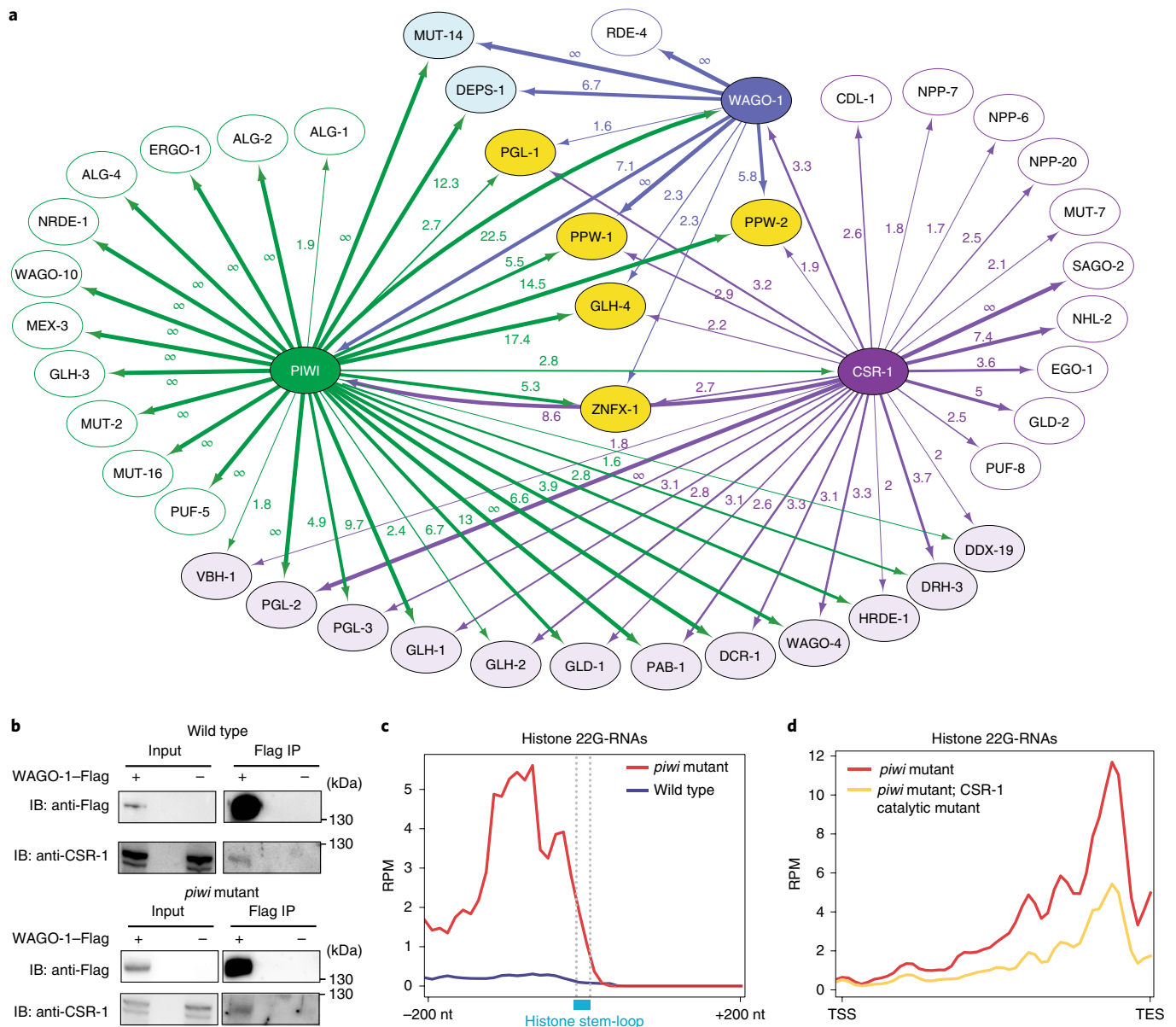


Fig. 4 | The CSR-1 pathway triggers the biogenesis of histone 22G-RNAs in *piwi* mutant worms. **a**, Network interactome map showing the overlap between CSR-1, PIWI- and WAGO-1-interacting proteins using MS. Only a selection of interacting proteins is shown, corresponding to known germ-granule components, RNAi factors and argonaute proteins. Proteins interacting with CSR-1, PIWI and CSR-1 are shown in yellow. Proteins interacting with only PIWI and WAGO are shown in blue. Proteins interacting with only CSR-1 and PIWI are shown in light violet. The numbers correspond to enrichment values in IPs, and proteins for which the peptides were detected exclusively in the IP but not in the control are indicated with an infinity symbol. **b**, Co-IP experiments in the wild-type (top) and *piwi*-mutant (bottom) lines, showing WAGO-1 interactions with CSR-1. The presence (+) or absence (-) of the tagged proteins is indicated. IP was performed using anti-Flag antibodies, and the blots were probed with anti-CSR-1 or anti-Flag antibodies. The amount of protein extract for IP was normalized to the total level of CSR-1 protein as mutant animals have less germline tissue (Extended Data Fig. 4e). The experiment was repeated independently twice with similar results. **c**, Metaprofile analysis showing the distribution of normalized 22G-RNA reads (RPM) 200 nucleotides upstream and 200 nucleotides downstream of the stem-loop sequence of histone mRNAs. The experiment was repeated independently twice with similar results. nt, nucleotides. **d**, Metaprofile analysis showing the distribution of normalized 22G-RNA reads (RPM) across histone genes in the *piwi*-mutant background with (yellow line) or without (red line) a mutation in the catalytic domain of CSR-1. TSS, transcriptional start site; TES, transcriptional end site. The experiment was repeated independently twice with similar results. Source data are available online.

promote RNA silencing across generations^{8,19,20,22,23}. PIWI and piRNAs might therefore help to initiate the formation of the piRNA-induced silencing complex in germ granules. To study whether the interactions between the downstream components of the piRNA-induced silencing complex are perturbed after removal of PIWI proteins, we quantified WAGO-1-interacting proteins using MS in wild-type worms compared with three progressive generations of

piwi-mutants. Our analysis revealed that the interactions between WAGO-1 and germ-granule components gradually diminished across generations in the absence of the PIWI protein (Fig. 3a,b). Instead, WAGO-1 interaction with some argonaute proteins, such as PPW-1 and the WAGO-1-interacting 22G-RNA biogenesis factor RDE-12 (ref. 35), was maintained even in late generations of *piwi*-mutant worms (Fig. 3a,b). Taken together, these results

suggest that the loss of interaction between WAGO-1 and germ-granule components might affect the localization of WAGO-1. To test this hypothesis, we performed live imaging of WAGO-1 and the germ-granule component PGL-1 in wild-type and *piwi*-mutant worms. Live imaging of a CRISPR-Cas9 strain expressing WAGO-1-GFP in wild-type worms confirmed its predominant perinuclear germ-granule localization (Fig. 3c), as previously observed³⁵. However, in late generations of *piwi* mutant worms, WAGO-1 lost its germ-granule localization and remained mainly cytoplasmic (Fig. 3c). We confirmed these results with immunostaining experiments using a CRISPR-Cas9 WAGO-1-Flag strain in wild-type and *piwi*-mutant worms (Extended Data Fig. 3b). Live imaging of the germ-granule component PGL-1 in *piwi*-mutant worms showed that the loss of WAGO-1 germ-granule localization was not caused by the disruption of germ-granule assembly (Fig. 3c), as PGL-1 granules were still formed even in sterile animals (Extended Data Fig. 3c). Furthermore, live imaging of the argonaute protein CSR-1, which does not belong to the piRNA pathway, showed germ-granule and cytoplasmic localization in wild-type and *piwi*-mutant worms, indicating that the loss of germ-granule localization in *piwi*-mutant lines is specific to the WAGO-1 argonaute (Fig. 3c, Extended Data Fig. 3c).

The CSR-1 pathway triggers the biogenesis of histone 22G-RNAs.

The data presented so far suggest that, in the absence of PIWI, another RNAi pathway is responsible for triggering the biogenesis and loading of histone 22G-RNAs into WAGOs. The proteomic analysis of PIWI-interacting proteins revealed the interactions with the argonaute CSR-1 (Fig. 2a, Supplementary Table 1a), which is known to counteract piRNA-silencing on mRNAs^{36,37} and promote histone biogenesis³⁸. We confirmed this interaction using co-IP experiments with a Flag-tagged CRISPR-Cas9 strain of CSR-1 (Extended Data Fig. 4a). We also analysed CSR-1-interacting proteins using MS and found, in addition to known components of the CSR-1 pathway, interactions with PIWI and WAGO-1 and many of their RNAi- and germ-granule-interacting proteins (Fig. 4a, Extended Data Fig. 4d, Supplementary Table 1c). However, some germ-granule components, such as DEPS-1, appear to specifically interact with only PIWI and WAGO-1 (Fig. 4a, Extended Data Fig. 4a,b). Nonetheless, the piRNA and the CSR-1 pathways shared many interactors (Fig. 4a), including WAGO-1, and—in the absence of PIWI—WAGO-1 might preferentially interact with CSR-1 in the cytoplasm. To confirm this hypothesis, using co-IP experiments, we found that WAGO-1 interacts with CSR-1 in *piwi*-mutant worms (Fig. 4b, Extended Data Fig. 4e), even though these mutant animals have lost WAGO-1 germ-granule localization and have reduced germline tissue and decreased levels of WAGO-1 compared with wild-type worms (Fig. 3c, Extended Data Fig. 4c,e). CSR-1 is known to bind to histone mRNAs and is thought to participate in the cleavage of the 3' end of histone mRNAs³⁸ together with its interacting stem-loop binding protein CDL-1 (ref. ³⁹; Fig. 4a, Extended Data Fig. 4d). Metaprofile analysis of histone 22G-RNAs in *piwi*-mutant worms showed a strong bias towards the end of the histone genes (Extended Data Fig. 4f), immediately upstream of the location of the stem-loop structure bound by CDL-1 (Fig. 4c). Thus, in the absence of PIWI, the cleavage of the 3' end of histone mRNA by CSR-1 and CDL-1 may trigger the production of histone 22G-RNAs loaded into WAGO-1. To test this hypothesis, we mutated the catalytic domain of CSR-1 using CRISPR-Cas9 and crossed this strain with the *piwi*-mutant strain. We observed a substantial reduction of histone 22G-RNAs in *piwi*-mutant animals, in which the catalytic activity of CSR-1 was zygotically abolished (Fig. 4d). Similar results were obtained by targeting *csr-1* with RNAi treatment in the *piwi*-mutant worms (Extended Data Fig. 4g). Moreover, RNAi treatment of *cdl-1* resulted in a slight reduction of 22G-RNAs in the region corresponding to the location of the stem-loop structure, and a

spreading of 22G-RNAs along the coding region towards the 5' end (Extended Data Fig. 4h). These results suggest that the interactions between CSR-1 and CDL-1 help to focus the cleavage activity of CSR-1 in proximity of the stem loop structure, and this triggers the synthesis and loading of histone 22G-RNAs into the WAGO pathway in the absence of PIWI.

Inactivation of downstream components of the piRNA pathway restores histone expression and fertility in *piwi*-mutant worms.

To determine whether the histone 22G-RNAs cause the transgenerational loss of fertility in piRNA mutant worms, we set out to rescue the fertility defects by inactivating the downstream piRNA factors that are responsible for producing 22G-RNAs. MUT-16 is one of the biogenesis factors that promotes the synthesis of 22G-RNAs loaded into WAGOs⁴⁰ and interacts with PIWI (Fig. 2a). RNAi depletion of MUT-16 (Fig. 5a) over two generations restored the fertility of *piwi*-mutant worms (Fig. 5b), and *piwi*-mutant worms that were treated continuously with *mut-16* RNAi did not become sterile (Extended Data Fig. 5a,b). Furthermore, *mut-16* RNAi treatment in sterile *piwi*-mutant worms was sufficient to restore their fertility. RNAi depletion of WAGO-1 also restored the fertility of sterile *piwi*-mutant worms (Fig. 5g). However, after RNAi depletion of WAGO-1, the restored fertility was lower compared with the *mut-16* RNAi treatment, suggesting that other argonaute proteins might participate in histone mRNA silencing in *piwi*-mutant animals (Fig. 5g). Indeed, RNAi treatment of *ppw-1* or *ppw-2*—the two other argonautes that interact with CSR-1, PIWI and WAGO-1 (Fig. 4a)—rescued the fertility of *piwi*-mutant worms (Extended Data Fig. 5c,d). RNAi knockdown of HRDE-1 did not recover fertility in *piwi*-mutant lines, probably because histone mRNAs are mainly silenced at the post-transcriptional level (Extended Data Fig. 5c,d). To demonstrate that the recovered fertility in *mut-16*-RNAi-treated animals was specifically promoted by the desilencing of histone mRNAs, we analysed 22G-RNAs and mRNAs using RNA-seq. The reduction of histone 22G-RNAs was correlated with increased expression of the replicative histone mRNAs in *mut-16*-RNAi-treated animals (Fig. 5c,d). Five piRNA-dependent targets showed a modest resiliencing signature, suggesting that they were unlikely to contribute to the recovered fertility (Extended Data Fig. 5e). An absence of resiliencing of REs was observed after *mut-16* RNAi treatment in the *piwi*-mutant background (Fig. 5e). The rescued fertility of piRNA mutants treated with *mut-16* RNAi was instead accompanied by further desilencing of REs (Fig. 5e, Extended Data Fig. 5f). Moreover, WAGO-1 remained cytoplasmic in those fertile animals, suggesting that there was no restoration of the canonical WAGO-1 silencing complex in germ granules (Fig. 5f). Furthermore, interaction between WAGO-1 and CSR-1 persisted even in the absence of histone 22G-RNAs (Extended Data Fig. 4e), indicating that this interaction is upstream of histone 22G-RNA synthesis. Collectively, these results suggest that the removal of histone 22G-RNAs after *mut-16* RNAi treatment, and not the resiliencing of REs, restored the fertility of *piwi*-mutant worms.

Inheritance of *piwi*-mutant phenotype and histone 22G-RNAs in wild-type worms.

To test whether the inheritance of histone 22G-RNAs is sufficient to transmit a *piwi*-like phenotype in wild-type worms, we outcrossed *prg-1(n4357)* hermaphrodites with wild-type males (Fig. 6a). We used worms from later generations of the *piwi* mutants, which were almost completely sterile, to select individuals expressing high levels of histone 22G-RNAs (Fig. 6b). In 2 out of 5 crosses, we selected three heterozygote (+/−) F₁ lines in each cross, and propagated two F₂ homozygote (−/−) *prg-1(n4357)* mutants and one wild-type (+/+) animal from each line and analysed the brood of the F₃ progeny (Fig. 6b, Extended Data Fig. 6a–d). The homozygote *prg-1(n4357)* mutants remained almost completely sterile after the cross (Fig. 6b, Extended Data Fig. 6a,c). The homozygote wild-type

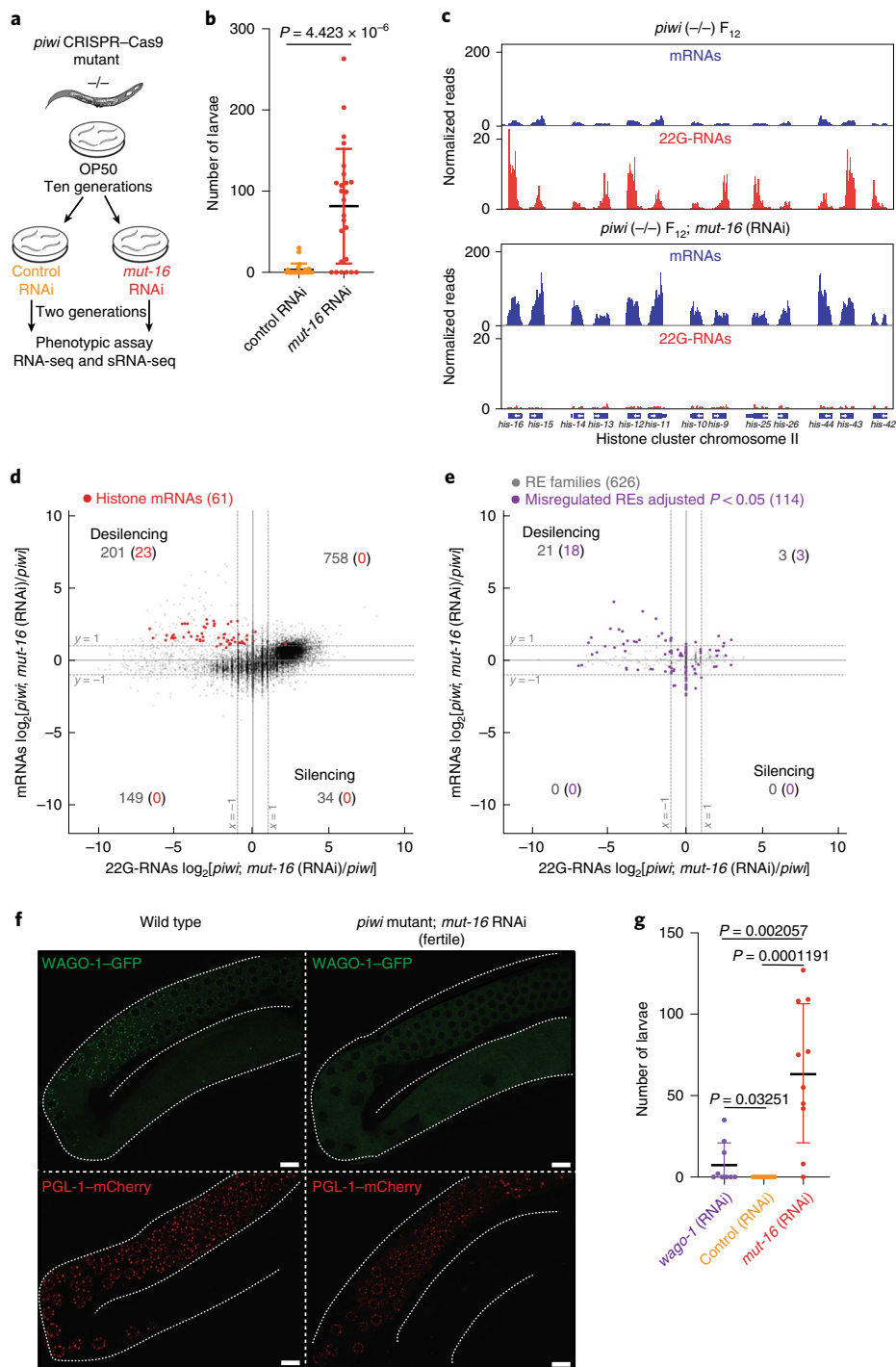


Fig. 5 | Removal of histone 22G-RNAs rescues *piwi* mutant transgenerational sterility. **a**, Schematic of the RNAi experiment using CRISPR-Cas9 *piwi*-mutant worms, grown for ten generations, on plates seeded with *Escherichia coli* OP50 and then shifted for two generations onto plates seeded with *mut-16* or control RNAi food. **b**, Results from a brood size assay of the experiment described in **a**. Each dot corresponds to the number of living larvae from individual worms. Data are mean \pm s.d. Statistical analysis was performed using two-tailed Mann-Whitney-Wilcoxon tests; $n = 25$ worms. **c**, Genomic view, similar to that shown in Fig. 1c, of one histone cluster in *piwi*-mutant F_{12} worms (top) or *piwi*-mutant F_{12} worms treated with *mut-16* RNAi (bottom). **d**, Comparison between mRNA and 22G-RNA \log_2 -transformed fold changes in *piwi*-mutant F_{12} worms treated with *mut-16* RNAi versus untreated *piwi*-mutant F_{12} worms. The dashed lines indicate twofold changes, and the number in parentheses indicates the portion of misregulated genes (twofold changes, adjusted $P < 0.05$, Wald test) belonging to the histone genes (red). The average from two biologically independent replicates is shown. **e**, The same comparison as shown in **d**, except that families of REs were analysed. The purple dots indicate significantly misregulated RE families by RNAi-seq (adjusted $P < 0.05$, Wald test). The average from two biologically independent replicates is shown. **f**, Live confocal images of WAGO-1-GFP and PGL-1-mCherry showing lack of WAGO-1 germ-granule localization in fertile *piwi*-mutant lines after *mut-16* RNAi treatment compared with the wild type. Scale bars, 10 μm . The experiment was repeated independently three times. **g**, Results from a brood size assay similar to the experiment described in **a**, except that sterile *piwi*-mutant worms were used for the assay. Each dot corresponds to the total number of living larvae from an individual worm. Data are mean \pm s.d. Statistical analysis was performed using two-tailed Mann-Whitney-Wilcoxon tests; $n = 10$ worms. Source data are available online.

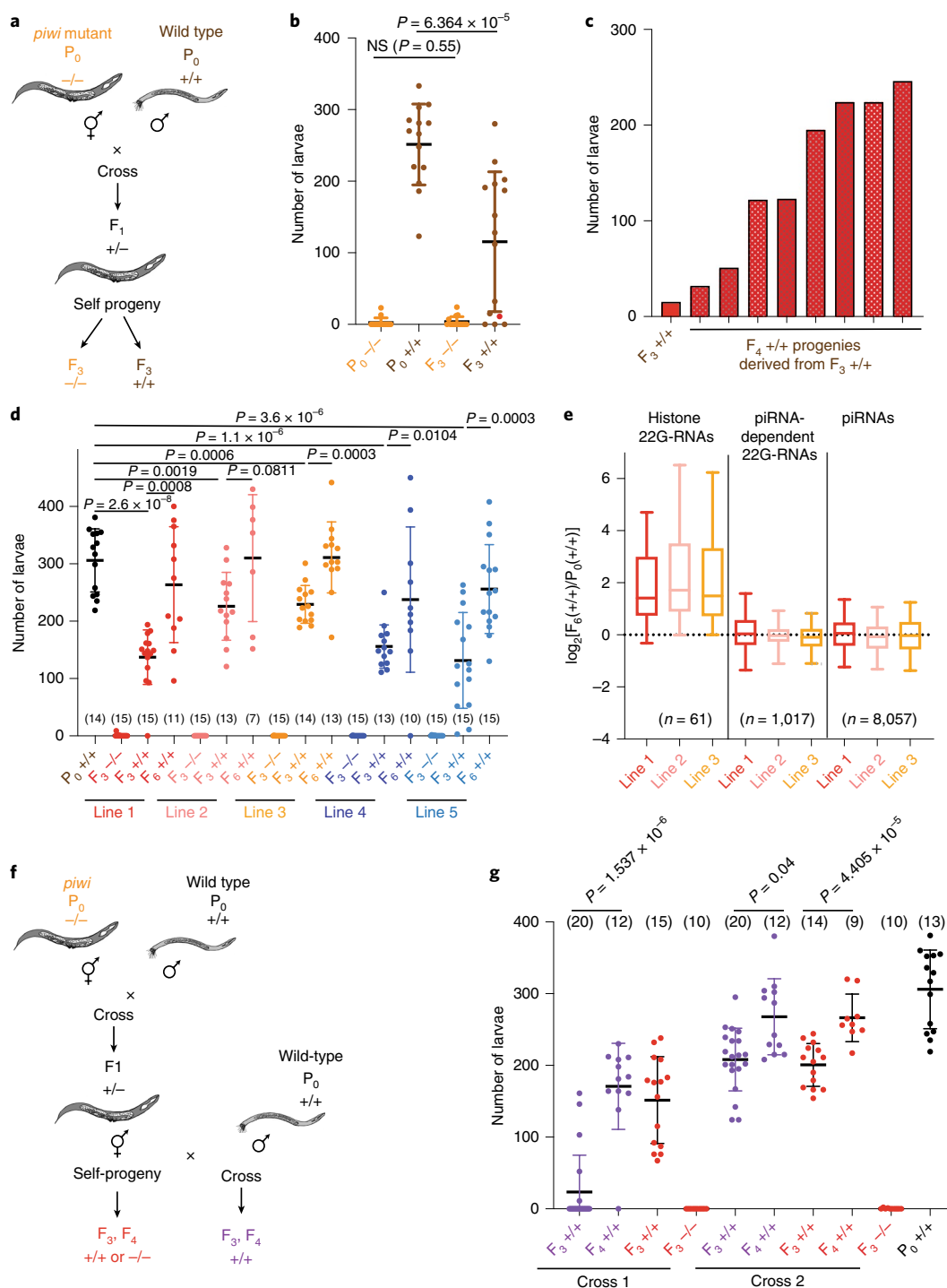


Fig. 6 | Histone 22G-RNAs facilitate the epigenetic inheritance of a piwi-like phenotype in wild-type worms. **a**, Schematic of a cross between wild-type males (+/+) and almost-sterile hermaphrodite *piwi*-mutant (*prg-1(4357)* or CRISPR-Cas9; -/-) worms. **b**, A brood size assay of the cross experiment described in **a**. Each dot corresponds to the number of living larvae from individual worms. Data are mean ± s.d. Statistical analysis was performed using two-tailed Mann-Whitney-Wilcoxon tests; *n* = 15 worms. **c**, Brood size assay as described in **b**, showing the brood of all of the individual *F*₄ +/+ animals (red bars) derived from the same *F*₃ +/+ parental worm (shown in **b** as a red dot). **d**, Brood size assay, as described in **b**, of the cross experiment described in **a**, using five selected *F*₂ wild-type crossed lines (+/+). Data are mean ± s.d.; the sample size *n* (worms) is indicated in parentheses. Statistical analysis was performed using two-tailed Mann-Whitney-Wilcoxon tests. **e**, The log₂-transformed fold change of sRNA in *F*₆ +/+ crossed line 1 (red), line 2 (pink) and line 3 (yellow) compared with the parental *P*₀ +/+. 22G-RNAs antisense to histone mRNAs, piRNA-dependent mRNA targets and piRNAs are shown. The line indicates the median value, the box indicates the first and third quartiles, and the whiskers indicate the 5th and 95th percentiles. The number of genes in each category is indicated in parentheses. **f**, Schematic of a cross between wild-type males (+/+) and hermaphrodite heterozygote *piwi*-mutant worms (+/-) (purple) or self-progeny (red). After the cross, wild-type (+/+) lines or self-crossed wild-type (+/+) and *piwi*-mutant (-/-) lines were selected. Wild-type (+/+) lines were propagated for two generations (*F*₃-*F*₄). **g**, A brood size assay, as described in **b**, of the cross experiment described in **f**. Data are mean ± s.d. Statistical analysis was performed using two-tailed Mann-Whitney-Wilcoxon tests; sample size *n* (worms) is indicated in parentheses. Source data are available online.

(+/+) animals displayed a *piwi*-like phenotype, showing reduced fertility compared with the parental P₀ wild-type worms (Fig. 6b, Extended Data Fig. 6a,c). To determine whether this reduced fertility was caused by inherited DNA mutations, we performed a brood size assay on all of the progeny from one of the most affected F₃ worms. All of the resulting F₄ animals showed increased fertility compared with the parental F₃ animal (Fig. 6c), indicating that DNA mutation was not responsible for the observed phenotype in the outcrossed wild-type worms. To further exclude possible genetic effects of the parental *prg-1(n4357)* mutant allele, we repeated the outcross experiment (Fig. 6a) using one of the *piwi*-mutant alleles generated by CRISPR–Cas9, and observed the same results (Fig. 6d, Extended Data Fig. 6e). Furthermore, we propagated the selected outcrossed homozygote wild-type lines for three subsequent generations and observed a gradual recovery of fertility (Fig. 6d), even though some wild-type lines did not completely recover the parental level of fertility. Sequencing 22G-RNAs from three of the outcrossed homozygote wild-type lines after six generations revealed that histone 22G-RNAs were inherited (Fig. 6e). We also crossed heterozygote hermaphrodite animals with wild-type males, and we observed a similar inherited phenotype in wild-type worms (Fig. 6f,g, Extended Data Fig. 6f). On the basis of these results, we propose that the maternal transmission of a pool of histone 22G-RNAs into wild-type worms can epigenetically affect their fertility.

Discussion

Here we have revealed the epigenetic mechanism that underlies the transgenerational loss of fertility in *C. elegans* piRNA mutants. We have shown that the *piwi* phenotype is not related to the role of piRNAs in repressing REs, but results from the inheritance of a pool of 22G-RNAs that are antisense to histone mRNAs, leading to the post-transcriptional silencing of all of the replicative histone genes. Previous reports have proposed that the sterility of *piwi* mutants is a consequence of ‘heritable stress’ caused by the derepression of REs, which leads to a form of adult diapause in late generations of *piwi*-mutant worms^{6,41}. Our RNA-seq analysis of almost 60,000 individual REs has shown that less than 100 REs are upregulated in *piwi*-mutant lines across generations, and their upregulation does not correlate with the sterility phenotype. Instead, we have documented the transgenerational silencing of histone mRNAs by 22G-RNAs, which causes a reduction in the pool of histone proteins and lack of incorporation of histones into the chromatin. The lack of histone incorporation into chromatin and defects in chromosome compaction can explain the reported cell death and germ cell atrophy in sterile *piwi*-mutant animals⁴¹. Thus, we propose that the inheritance of histone 22G-RNAs underlies the heritable stress that ultimately leads to sterile animals.

Our results show that the silencing of histone genes is caused by redirecting the WAGO pathway away from piRNA-dependent 22G-RNA targets to histone mRNAs. This process requires several worm generations, possibly because the WAGO pathway can still be recruited to piRNA-dependent 22G-RNA targets in the absence of PIWI for several generations. We speculate that the germ-granule localization of WAGO-1—as well as its interaction with specific germ-granule components, such as DEPS-1—helps to maintain the piRNA-induced WAGO-1 silencing complex on piRNA targets, even in the absence of PIWI for certain generations. However, the interaction between WAGO-1 and DEPS-1 might not be stable without PIWI, and WAGO-1 interaction with CSR-1 might be favoured in the cytoplasm allowing the WAGO-1 silencing complex to localize on histone mRNAs. In support of this hypothesis, we have shown that the interaction of WAGO-1 with germ-granule components is gradually decreased across generations of *piwi*-mutant animals, even though it is still capable of interacting in the cytoplasm with the 22G-RNA biogenesis factor RDE-12 and the argonaute CSR-1. In addition to WAGO-1, other downstream argonautes of the

piRNA pathway might relocate to histone mRNAs in the absence of PIWI. We have shown that two of these argonautes—PPW-1 and PPW-2, which also interact with CSR-1 in wild-type worms—are required for histone mRNA silencing in *piwi*-mutant worms, suggesting that they might also relocate on histone mRNAs, similar to WAGO-1.

Our results suggest that the cleavage of histone pre-mRNAs by CSR-1 is required to facilitate the synthesis and loading of histone 22G-RNAs by the WAGO pathway in the absence of PIWI. CSR-1 may also cleave other germline mRNA targets¹². However, we did not observe silencing of CSR-1 mRNA targets by the WAGO pathway in *prg-1*-mutant lines. One possibility is that the amount of cleavage product from CSR-1 mRNA targets is much lower than the cleaved histone mRNAs. Alternatively, other factors, such as mRNA-specific nucleotide sequences^{18,43}, may prevent germline mRNAs from becoming targets of the WAGO pathway in the absence of piRNAs.

Our results, together with previous reports^{28,29}, suggest that piRNAs might be required to only initiate, and not to maintain, the silencing of REs. Nonetheless, continuous synthesis of piRNAs is required in each generation to repress potential RE invasions. We speculate that the piRNA-driven production of WAGO-bound 22G-RNAs, which we observed against more than a thousand of protein-coding genes, functions to maintain the piRNA-induced silencing complex in readiness to silence foreign RNAs. However, it is unclear how the piRNA pathway can be evolutionary retained if it is only waiting for a potential invasion. Previous studies have shown the physiological function of PIWI in regulating some germline mRNA targets^{44,45}. On the basis of our results, we propose a model in which the coupling between the lack of piRNAs and the consequent silencing of histone genes, initiated by CSR-1 and CDL-1, acts as an evolutionary force that maintains a functional piRNA-induced silencing pathway (Extended Data Fig. 7). Thus, the processing of histone mRNAs by CSR-1 and the co-evolution and co-existence of both the piRNA and the CSR-1 pathways could be an important evolutionary force in retaining the piRNA pathway in some nematode lineages. Indeed, nematode clades that have lost the piRNA pathway also lack CSR-1 (ref. 46), except for clade III nematodes⁴⁷, which retain the CSR-1 pathway. We speculate that clade III nematodes escaped the sterility phenotype because they have polyadenylated histone mRNAs⁴⁸, which probably do not require CSR-1 and CDL-1 for processing.

We have observed the transmission of a *piwi*-like phenotype in wild-type worms through sRNAs. These results implicate sRNAs as molecules that are capable of transmitting epigenetic information between individuals and across generations, over and above the information encoded in their genomes.

Online content

Any methods, additional references, Nature Research reporting summaries, source data, extended data, supplementary information, acknowledgements, peer review information; details of author contributions and competing interests; and statements of data and code availability are available at <https://doi.org/10.1038/s41556-020-0462-7>.

Received: 9 April 2019; Accepted: 5 January 2020;

Published online: 3 February 2020

References

- Ozata, D. M., Gainetdinov, I., Zoch, A., O’Carroll, D. & Zamore, P. D. PIWI-interacting RNAs: small RNAs with big functions. *Nat. Rev. Genet.* **20**, 89–108 (2019).
- Thomson, T. & Lin, H. The biogenesis and function of PIWI proteins and piRNAs: progress and prospect. *Annu. Rev. Cell Dev. Biol.* **25**, 355–376 (2009).
- Tóth, K. F., Pezic, D., Stuwe, E. & Webster, A. The piRNA pathway guards the germline genome against transposable elements. *Adv. Exp. Med. Biol.* **886**, 51–77 (2016).

4. Wu, P.-H. et al. An evolutionarily conserved piRNA-producing locus required for male mouse fertility. Preprint at *bioRxiv* <https://doi.org/10.1101/386201> (2018).
5. Gou, L. T. et al. Ubiquitination-deficient mutations in human Piwi cause male infertility by impairing histone-to-protamine exchange during spermiogenesis. *Cell* **169**, 1090–1104 (2017).
6. Simon, M. et al. Reduced insulin/IGF-1 signaling restores germ cell immortality to *Caenorhabditis elegans* Piwi mutants. *Cell Rep.* **7**, 762–773 (2014).
7. Katz, D. J., Edwards, T. M., Reinke, V. & Kelly, W. G. A *C. elegans* LSD1 demethylase contributes to germline immortality by reprogramming epigenetic memory. *Cell* **137**, 308–320 (2009).
8. Buckley, B. A. et al. A nuclear argonaute promotes multigenerational epigenetic inheritance and germline immortality. *Nature* **489**, 447–451 (2012).
9. Frézal, L., Demoinet, E., Braendle, C., Miska, E. & Félix, M.-A. Natural genetic variation in a multigenerational phenotype in *C. elegans*. *Curr. Biol.* **28**, 2588–2596 (2018).
10. Spracklin, G. et al. The RNAi inheritance machinery of *Caenorhabditis elegans*. *Genetics* **206**, 1403–1416 (2017).
11. Perez, M. F. & Lehner, B. Intergenerational and transgenerational epigenetic inheritance in animals. *Nat. Cell Biol.* **21**, 143–151 (2019).
12. Batista, P. J. et al. PRG-1 and 21U-RNAs interact to form the piRNA complex required for fertility in *C. elegans*. *Mol. Cell* **31**, 67–78 (2008).
13. Ruby, J. G. et al. Large-scale sequencing reveals 21U-RNAs and additional microRNAs and endogenous siRNAs in *C. elegans*. *Cell* **127**, 1193–1207 (2006).
14. Das, P. P. et al. Piwi and piRNAs act upstream of an endogenous siRNA pathway to suppress Tc3 transposon mobility in the *Caenorhabditis elegans* germline. *Mol. Cell* **31**, 79–90 (2008).
15. Cecere, G., Zheng, G. X. Y., Mansisidor, A. R., Klymko, K. E. & Grishok, A. Promoters recognized by forkhead proteins exist for individual 21U-RNAs. *Mol. Cell* **47**, 734–745 (2012).
16. Gu, W. et al. CapSeq and CIP-TAP identify Pol II start sites and reveal capped small RNAs as *C. elegans* piRNA precursors. *Cell* **151**, 1488–1500 (2012).
17. Shen, E. Z. et al. Identification of piRNA binding sites reveals the argonaute regulatory landscape of the *C. elegans* germline. *Cell* **172**, 937–951 (2018).
18. Zhang, D. et al. The piRNA targeting rules and the resistance to piRNA silencing in endogenous genes. *Science* **359**, 587–592 (2018).
19. Lee, H. C. et al. *C. elegans* piRNAs mediate the genome-wide surveillance of germline transcripts. *Cell* **150**, 78–87 (2012).
20. Bagijn, M. P. et al. Function, targets, and evolution of *Caenorhabditis elegans* piRNAs. *Science* **337**, 574–578 (2012).
21. Hourri-Ze'evi, L. et al. A tunable mechanism determines the duration of the transgenerational small RNA inheritance in *C. elegans*. *Cell* **165**, 88–99 (2016).
22. Spracklin, G. et al. The RNAi inheritance machinery of *Caenorhabditis elegans*. *Genetics* **206**, 1403–1416 (2017).
23. Wan, G. et al. Spatiotemporal regulation of liquid-like condensates in epigenetic inheritance. *Nature* **557**, 679–683 (2018).
24. Zeller, P. et al. Histone H3K9 methylation is dispensable for *Caenorhabditis elegans* development but suppresses RNA:DNA hybrid-associated repeat instability. *Nat. Genet.* **48**, 1385–1395 (2016).
25. McMurchy, A. N. et al. A team of heterochromatin factors collaborates with small RNA pathways to combat repetitive elements and germline stress. *eLife* **6**, e21666 (2017).
26. Ni, J. Z., Chen, E. & Gu, S. G. Complex coding of endogenous siRNA, transcriptional silencing and H3K9 methylation on native targets of germline nuclear RNAi in *C. elegans*. *BMC Genom.* **15**, 1157 (2014).
27. Shirayama, M. et al. piRNAs initiate an epigenetic memory of nonself RNA in the *C. elegans* germline. *Cell* **150**, 65–77 (2012).
28. de Albuquerque, B. F. M., Placentino, M. & Ketting, R. F. Maternal piRNAs are essential for germline development following de novo establishment of endo-siRNAs in *Caenorhabditis elegans*. *Dev. Cell* **34**, 448–456 (2015).
29. Phillips, C. M., Brown, K. C., Montgomery, B. E., Ruvkun, G. & Montgomery, T. A. piRNAs and piRNA-dependent siRNAs protect conserved and essential *C. elegans* genes from misrouting into the RNAi pathway. *Dev. Cell* **34**, 457–465 (2015).
30. Weick, E. M. et al. PRDE-1 is a nuclear factor essential for the biogenesis of ruby motif-dependent piRNAs in *C. elegans*. *Genes Dev.* **28**, 783–796 (2014).
31. Pettitt, J., Crombie, C., Schümperli, D. & Müller, B. The *Caenorhabditis elegans* histone hairpin-binding protein is required for core histone gene expression and is essential for embryonic and postembryonic cell division. *J. Cell Sci.* **115**, 857–866 (2002).
32. Kodama, Y., Rothman, J. H., Sugimoto, A. & Yamamoto, M. The stem-loop binding protein CDL-1 is required for chromosome condensation, progression of cell death and morphogenesis in *Caenorhabditis elegans*. *Development* **129**, 187–196 (2002).
33. Gu, W. et al. Distinct argonaute-mediated 22G-RNA pathways direct genome surveillance in the *C. elegans* germline. *Mol. Cell* **36**, 231–244 (2009).
34. Spike, C. A., Bader, J., Reinke, V. & Strome, S. DEPS-1 promotes P-granule assembly and RNA interference in *C. elegans* germ cells. *Development* **135**, 983–993 (2008).
35. Shirayama, M., Stanney, W., Gu, W., Seth, M. & Mello, C. C. The vasa homolog RDE-12 engages target mRNA and multiple argonaute proteins to promote RNAi in *C. elegans*. *Curr. Biol.* **24**, 845–851 (2014).
36. Wedeles, C. J., Wu, M. Z. & Claycomb, J. M. Protection of germline gene expression by the *C. elegans* argonaute CSR-1. *Dev. Cell* **27**, 664–671 (2013).
37. Seth, M. et al. The *C. elegans* CSR-1 argonaute pathway counteracts epigenetic silencing to promote germline gene expression. *Dev. Cell* **27**, 656–663 (2013).
38. Avgousti, D. C., Palani, S., Sherman, Y. & Grishok, A. CSR-1 RNAi pathway positively regulates histone expression in *C. elegans*. *EMBO J.* **31**, 3821–3832 (2012).
39. Keall, R., Whitelaw, S., Pettitt, J. & Müller, B. Histone gene expression and histone mRNA 3' end structure in *Caenorhabditis elegans*. *BMC Mol. Biol.* **8**, 51 (2007).
40. Zhang, C. et al. *mut-16* and other mutator class genes modulate 22G and 26G siRNA pathways in *Caenorhabditis elegans*. *Proc. Natl Acad. Sci. USA* **108**, 1201–1208 (2011).
41. Heestand, B., Simon, M., Frenk, S., Titov, D. & Ahmed, S. Transgenerational sterility of Piwi mutants represents a dynamic form of adult reproductive diapause. *Cell Rep.* **23**, 156–171 (2018).
42. Gerson-Gurwitz, A. et al. A small RNA-catalytic argonaute pathway tunes germline transcript levels to ensure embryonic divisions. *Cell* **165**, 396–409 (2016).
43. Seth, M. et al. The coding regions of germline mRNAs confer sensitivity to argonaute regulation in *C. elegans*. *Cell Rep.* **22**, 2254–2264 (2018).
44. Tang, W. et al. A sex chromosome piRNA promotes robust dosage compensation and sex determination in *C. elegans*. *Dev. Cell* **44**, 762–770 (2018).
45. Barberán-Soler, S. et al. Co-option of the piRNA pathway for germline-specific alternative splicing of *C. elegans* TOR. *Cell Rep.* **8**, 1609–1616 (2014).
46. Sarkies, P. et al. Ancient and novel small RNA pathways compensate for the loss of piRNAs in multiple independent nematode lineages. *PLoS Biol.* **13**, e1002061 (2015).
47. Tu, S. et al. Comparative functional characterization of the CSR-1 22G-RNA pathway in *Caenorhabditis* nematodes. *Nucleic Acids Res.* **43**, 208–224 (2015).
48. Wyler-Duda, P., Bernard, V., Stadler, M., Suter, D. & Schümperli, D. Histone H4 mRNA from the nematode *Ascaris lumbricoides* is cis-spliced and polyadenylated. *Biochim. Biophys. Acta* **1350**, 259–261 (1997).

Publisher's note Springer Nature remains neutral with regard to jurisdictional claims in published maps and institutional affiliations.

© The Author(s), under exclusive licence to Springer Nature Limited 2020

Methods

Strains of *C. elegans*. Strains were maintained at 20 °C using standard methods⁴⁹. The wild-type reference strain used was Bristol N2. A complete list of the strains used in this study is provided in Supplementary Table 2.

Generation of CRISPR–Cas9 lines. CRISPR–Cas9 alleles were generated by microinjecting Cas9–guide RNA (gRNA) ribonucleoprotein complexes into hermaphrodite gonads as described previously⁵⁰.

gRNA in vitro transcription, repair templates and microinjection. Unique and specific gRNA sequences were selected using the off-target prediction CRISPR design tool at <https://crispr.mit.edu/>. Gene-specific gRNA sequences were included in a 60-nucleotide forward oligo, which contained a 22-nucleotide T7 promoter sequence followed by the 20-nucleotide gene-specific gRNA sequence and a 18-nucleotide sequence with homology to the 5' tracrRNA scaffold sequence included in the AP0905 plasmid (provided by the laboratory of G. Seydoux). This forward oligo was used in combination with a reverse oligo homologous to the 3' sequence of the tracrRNA to amplify, using PCR from the AP0905 plasmid, a double-stranded DNA template for gRNA in vitro transcription. PCR reactions were performed using High-Fidelity Phusion DNA Polymerase (Thermo Fisher Scientific) and the PCR products were purified using the DNA clean and concentrator kit (Zymo Research). gRNAs were transcribed in vitro for 3 h at 37 °C from approximately 400 ng of template PCR products using the T7 RNA polymerase kit (New England Biolabs) following the manufacturer's instructions. In vitro transcribed RNAs were treated with DNase using 2 U of Turbo DNase (Ambion) and then purified using the RNA clean and concentrator kit (Zymo Research). For single-nucleotide modifications or small tag edits, we used single-stranded oligonucleotides containing homology arms of approximately 33 bp as repair templates, ordered from IDT, as standard 4 nM ultramer oligos. In the case of larger edits, such as fluorescent protein tag sequences, we generated double-stranded DNA repair templates by amplifying eGFP or mCherry from PJJR82 and PJJR83 plasmids (provided by the laboratory of M. Boxem) by PCR using specific oligos containing homology arms of approximately 33 bp. Silent mutations were included where necessary in the repair templates to modify either the PAM sequence or the gRNA seed region to prevent Cas9 from cleaving the repair template. To improve screening efficiency, a gRNA targeting *dpy-10* was used as a co-CRISPR marker as described previously⁵¹. Injection mixes were prepared as described previously⁵⁰.

In brief, 10 µl mixes typically contained the following: 10–15 µM Cas9-NLS protein (Institut Pasteur core facility), 300 ng µl⁻¹ in vitro transcribed *dpy-10* gRNA, 1 µg µl⁻¹ in vitro transcribed target-gene gRNA, 0.44 pmol µl⁻¹ of *dpy-10* single-stranded oligodeoxynucleotide (ssODN) repair template and 0.8 pmol µl⁻¹ of target-gene ssODN repair template or 300 ng µl⁻¹ target-gene double-stranded DNA repair template.

Screening and validation of CRISPR–Cas9 alleles. Modified target loci were screened by PCR using target-gene-specific oligos. To generate the *piwi* mutant, we introduced a STOP codon (UAG) followed by a NheI restriction site after the 5th codon of *prg-1*. We selected this region because it contained a PAM sequence that enabled us to specifically target *prg-1* and not *prg-2*, which is a gene with high sequence homology to *prg-1*. Primers specific to *prg-1* were used to amplify the genomic region spanning the edited locus, and a restriction enzyme digestion was performed on the PCR amplicon. After digestion with NheI, the wild-type allele produces an 889-nucleotide band whereas the edited fragments produce two bands (616 nucleotides + 275 nucleotides). We used the same gRNA to introduce a 3×Flag::2×HA epitope tag after the 6th codon of *prg-1*. Similarly, we used a *csr-1*-specific gRNA to introduce a 3×Flag::1×HA epitope tag after the first codon of the short isoform of CSR-1 to tag both the long and the short isoforms of the protein. We used the 3×Flag::HA::CSR-1 strain as an entry strain to introduce mCherry to create a fluorescently tagged mCherry::3×Flag::HA::CSR-1 strain. We also introduced a 3×Flag::OLLAS tag immediately after the start codon of *wago-1*. Owing to the high sequence homology between *wago-1* and *wago-2* we were unable to find a completely specific *wago-1* gRNA close to the start codon. We used a gRNA that targets both *wago-1* and *wago-2* and designed gene-specific primers to screen for worms in which only *wago-1* was edited. To control for unwanted modifications at the *wago-2* locus, we sequenced the *wago-2*-targeted region and confirmed the absence of any type of edit. Similar to the mCherry-tagged version of CSR-1, we used the 3×Flag::OLLAS::WAGO-1 strain as an entry strain to introduce eGFP into the 3×Flag::OLLAS region to obtain a fluorescently tagged 3×Flag::GFP::OLLAS::WAGO-1 strain. To generate a catalytic-dead mutant of *csr-1*, we substituted a conserved aspartic acid residue with an alanine residue (D769A), a modification that was previously shown to be sufficient to abolish the catalytic activity of CSR-1 in vitro⁵².

The nucleotide changes introduced to modify the codon in addition to the silent changes added to the repair removed a MaeII restriction site in our *csr-1*(D769A) edited locus. We screened for the presence of our edit in PCR products on the basis of resistance to restriction using MaeII. All of the loci edited in this study were verified by sequencing locus-specific PCR products. A detailed list of gRNAs, single-stranded DNA and double-stranded DNA repair templates and primers used for genotyping is provided in Supplementary Table 3.

Balancers and genetics. *csr-1*(D769A) mutants were balanced into nT1[qIs51], a reciprocal translocation between chromosome IV and V containing a recessive lethal marker that causes embryonic lethality of homozygous balanced worms. Furthermore, nT1[qIs51] carries a balancer-associated dominant unc phenotype and GFP transgenes that enable the visual identification of heterozygous animals⁵³.

We used a COPAS Biosorter (Union Biometrica) to set up a fluorescence-based sorting approach that enabled us to obtain large synchronized homozygous *csr-1*(D769A) populations for genome-wide analysis of sRNAs.

The *csr-1*(D769A) (IV)/nT1[qIs51] (IV;V);*piwi*/*piwi* (I) strain was obtained after a three-step crossing strategy summarized here as follows. First, wild-type males were mated with a single early-generation *piwi* mutant hermaphrodite. Second, the resulting F₁ *piwi*+ (I) males were mated with *csr-1*(D769A) (IV)/nT1[qIs51] (IV;V) balanced worms. The non-GFP males resulting from the crossed progeny of this second cross are *csr-1*(D769A)/+ (IV) and, in 50% of the cases, are *piwi*+ (I). Third, we pooled at least five of these non-GFP males and crossed them with *csr-1*(D769A) (IV)/nT1[qIs51] balanced worms to introduce the *piwi* allele in heterozygosis in the progeny. We screened for GFP positive (/nT1[qIs51] balanced) F₁ worms from this cross carrying either *csr-1* wild type or the *csr-1*(D769A) allele and the *piwi*+ mutation. From these two different lines, we singled out GFP balanced progeny individuals to finally obtain the *csr-1*(D769A) (IV)/nT1[qIs51] (IV;V);*piwi*/*piwi* (I) and their corresponding control +/+ /nT1[qIs51] (IV;V);*piwi*/*piwi* (I) animals.

Genotyping. For genotyping, single worms were manually picked in 20 µl of worm lysis buffer (30 mM Tris pH 8, 8 mM EDTA, 100 mM NaCl, 0.7% NP-40, 0.7% Tween 20) containing 100 µg ml⁻¹ proteinase K. The solution was incubated at 65 °C for 1 h, then the proteinase K was inactivated at 95 °C for 15 min. A fraction of the lysate (5 µl) was used as template for a PCR reaction using gene-specific oligos. The sequences of primers used for genotyping are provided in Supplementary Table 3.

Crossing/mating experiments using *piwi*-mutant worms. Crossing experiments were performed on Petri dishes (2.5 cm) seeded with OP50 *E. coli* food using one hermaphrodite *piwi*-mutant worm at young-adult stage together with around five wild-type males. The efficiency of the cross was assessed by the percentage of F₁ males that were present in the progeny. For each experiment, at least five crosses were set up, and the best three were selected on the basis of male incidence criteria. For each cross, five F₁ hermaphrodite L4 larvae were transferred onto individual plates and genotyped after egg laying to screen for heterozygous *piwi*+ animals. F₂ larvae from *piwi* heterozygote F₁ animals were individually grown and genotyped to obtain wild-type and *piwi*-homozygous mutant lines.

Brood size assays. Manually picked L1 larvae were grown individually on Petri dishes (2.5 cm) seeded with OP50 *E. coli* food until adulthood, and were then transferred onto a new plate every 24 h for a total of 3 d. The brood size of each worm was scored by counting the total number of larvae laid on the three plates. For each brood size experiment, at least 15 worms were scored for each strain.

RNAi experiments. RNAi clones used in this study were obtained from the Ahringer library⁵⁴. An empty vector (L4440) was used as a control in all of our RNAi experiments. RNAi experiments for brood size assays were performed using manually picked L1 larvae grown on Petri dishes (2.5 cm) seeded with bacteria-producing double-stranded RNA complementary to the gene of interest or control empty vector. RNAi experiments for RNA extraction were performed using Petri dishes (15 cm) seeded with concentrated RNAi food.

RNA extraction. Synchronous populations of worms were grown at 20 °C on nematode growth medium plates seeded with OP50 *E. coli* concentrated food at a density of maximum 40,000 animals per Petri dish (15 cm) and collected at young-adult stage 48 h after hatching. The collected animals were washed three times with M9 buffer, and 40 µl of worm pellet was frozen in dry ice with TRI Reagent (MRC). After five repetitions of freeze and thaw, total RNA was isolated according to the TRI Reagent protocol. Then, 10 µg RNA was treated with 2 U Turbo DNase (Ambion) at 37 °C for 30 min followed by phenol extraction and isopropanol precipitation. An Agilent 2200 TapeStation System was used to evaluate the RIN indexes of all of the RNA preps, and only samples with RNA integrity number (RIN) > 8 were used for downstream applications. For the preparation of total RNA extracted from generation F₁ of wild-type and *piwi*-mutant worms, ten manually picked worms were used.

Strand-specific RNA-seq library preparation. DNase-treated total RNA with RIN > 8 was used to prepare strand-specific RNA libraries. We developed an RNase-H-based method to degrade *C. elegans* and mitochondrial ribosomal RNAs using 50-nucleotide oligos complementary to *C. elegans* rRNA and mitochondrial RNA sequences. The sequences of the oligos used are provided in Supplementary Table 4. DNase-treated total RNA (1 µg) was mixed with 1 µg of oligos at equimolar concentration and 1× probe hybridization buffer (200 mM NaCl, 10 mM Tris pH 7.5) and incubated in a thermocycler using the following parameters: 2 min at 95 °C followed by 0.1 °C s⁻¹ at 95–45 °C, and then held for 2 min at 45 °C. Next, 2 µl of ThermoStable RNase H (epicentre) was added to the reactions together with

1× RNase H reaction buffer (50 mM Tris pH 7.5, 100 mM NaCl, 10 mM MgCl₂) and incubated for 30 min at 45 °C. Digested RNAs were next treated with 2 U of Turbo DNase (Ambion) at 37 °C for 30 min followed by purification using 2.2 volumes of Agencourt RNAClean XP Beads (Beckman Coulter, NC0068576) following the manufacturer's instructions. Then, 100 ng of Ribosomal-depleted RNAs were used to generate strand-specific RNA libraries using NEBNext Ultra II Directional RNA Library Prep Kit for Illumina (E7760S). Multiplexed RNA libraries were quantified using the Qubit Fluorometer High Sensitivity dsDNA assay kit (Thermo Fisher Scientific, Q32851) and were sequenced on a NextSeq-500 Illumina platform using the NextSeq 500/550 High Output v2 kit 75 cycles (FC-404-2005).

sRNA-seq library preparation. Total RNA (10 µg) with RIN > 8 was used to generate sRNA libraries. The library preparation was performed essentially as described previously⁵⁵, except that a 5' polyphosphatase (Lucigen RP8092H) treatment was performed so that we were able to clone tri-phosphate sRNAs, and the PAGE gel extraction after each ligation was substituted with purification using 1.8 volumes of Agencourt RNAClean XP Beads (Beckman Coulter, NC0068576) and 3 volumes of isopropanol. The multiplexed amplified libraries were further purified using PippinPrep DNA size selection with 3% gel cassettes and the following parameters for the selection: BP start (115); BP end (165). The purified libraries were quantified using the Qubit Fluorometer High Sensitivity dsDNA assay kit (Thermo Fisher Scientific, Q32851) and sequenced with either a NextSeq-500 Illumina platform using the NextSeq 500/550 High Output v2 kit 75 cycles (FC-404-2005) or an Illumina MiniSeq platform using the MiniSeq High Output Reagent Kit 75 cycles (FC-420-1001).

GRO-seq. Global run-on sequencing (GRO-seq) experiments were performed as described previously⁵⁶, except that biotin-UTP was used to label nascent RNAs. Two biological replicates were generated using synchronous 40,000 wild-type and *prg-1(n4357)*-mutant worms collected 48 h after hatching.

IP for the co-IP or MS experiments. A synchronous population of 120,000 (for CSR-1, PRG-1 IPs) or 40,000 (for WAGO-1 IPs for MS) worms was collected 48 h after hatching and suspended in the extraction buffer (50 mM HEPES pH 7.5, 300 mM NaCl, 5 mM MgCl₂, 10% glycerol, 0.25% NP-40, protease inhibitor cocktails (Fermentas)) followed by 30 strokes using a metal dounce on ice. Crude protein extracts were centrifuged at 12,000 r.p.m. at 4 °C for 10 min. Protein concentration was quantified using the Bradford assay, and 2 mg of protein extract was incubated with 15 µl of packed anti-Flag M2 magnetic agarose beads (Sigma M8823) for 1 h at 4 °C. After four washes with the extraction buffer, the beads were resuspended with 2× NuPAGE LDS sample buffer (Thermo Fisher Scientific) for co-IP experiments or washed twice with 100 µl of 25 mM NH₄HCO₃ for MS. For the co-IP experiments shown in Fig. 4b and Extended Data Fig. 4e, the total-protein extract from *piwi*-mutant and control strains were normalized to the level of CSR-1 protein to avoid differences in the total germline proteins due to the reduced germline tissue in *piwi*-mutant strains.

MS. Digestion with 0.2 µg of trypsin/LysC (Promega) was performed on-beads derived from IP experiments for 1 h in 100 µl of 25 mM NH₄HCO₃. Samples were then loaded into a homemade C18 Stage Tips for desalting (principally, by stacking one 3M Empore SPE Extraction Disk Octadecyl (C18) and beads from SepPak C18 CartridgeWaters into a 200 µl micro pipette tip). Peptides were eluted using a ratio of 40:60 MeCN:H₂O + 0.1% formic acid and vacuum concentrated to dryness. Online chromatography was performed using an RSLCnano system (Ultimate 3000, Thermo Fisher Scientific) coupled to an Orbitrap Fusion Tribrid mass spectrometer (Thermo Fisher Scientific). Peptides were trapped in a C18 column (75 µm inner diameter × 2 cm; nanoViper Acclaim PepMap 100, Thermo Fisher Scientific) with buffer A (2:98 MeCN:H₂O in 0.1% formic acid) at a flow rate of 4.0 µl min⁻¹ over 4 min. Separation was performed using a 50 cm × 75 µm C18 column (nanoViper Acclaim PepMap RSLC, 2 µm, 100 Å, Thermo Fisher Scientific), regulated to a temperature of 55 °C with a linear gradient of 5% to 25% buffer B (100% MeCN in 0.1% formic acid) at a flow rate of 300 nl min⁻¹ over 100 min. Full-scan MS was acquired using an Orbitrap Analyzer with the resolution set to 120,000, and ions from each full scan were higher-energy C-trap dissociation (HCD) fragmented and analysed in the linear ion trap.

For identification, the data were searched against the *C. elegans* (CAEL) UP000001940 database using Sequest HF through Proteome Discoverer (v.2.1). Enzyme specificity was set to trypsin and a maximum of two missed cleavage sites were allowed. Oxidized methionine, N-terminal acetylation, phosphorylated serine/threonine/tyrosine and carbamidomethyl cysteine were set as variable modifications. Maximum allowed mass deviation was set to 10 ppm for monoisotopic precursor ions and 0.6 Da for MS/MS peaks.

The resulting files were further processed using myProMS⁵⁷ v.3.6 (work in progress). False-discovery rate (FDR) was calculated using Percolator and was set to 1% at the peptide level for the whole study. Label-free quantification was performed using peptide extracted ion chromatograms (XICs), computed with MassChroQ⁵⁸ v.2.2.2. For protein quantification, XICs from proteotypic peptides shared between compared conditions (TopN matching) with missed cleavages and some modification (carbamidomethyl cysteines) were used. Global median

absolute deviation (MAD) normalization was applied to the total signal to correct the XICs for each biological replicate. To estimate the significance of the change in protein abundance, a linear model (adjusted for peptides and biological replicates) was performed, and *P* values were FDR-adjusted using the Benjamini–Hochberg procedure with a control threshold set to 0.05. Cytoscape⁵⁹ was used to generate the interactome network map.

The MS proteomics data have been deposited to the ProteomeXchange Consortium via the PRIDE⁶⁰ partner repository with the dataset identifier PXD012557.

Western blotting. Protein extracts, prepared as described above, were resolved on precast NuPAGE Novex 4–12% Bis-Tris gels (Invitrogen, NP0321BOX). The proteins were transferred to a nylon membrane with the semidry transfer Pierce Power System (Thermo Fisher Scientific) using the preprogrammed method for high-molecular-mass protein. The primary antibodies used included anti-PRG-1 (ref. ⁶; a gift from the Mello laboratory), anti-CSR-1 (ref. ⁶¹), anti-PGL-1 (ref. ⁶²) and anti-DEPS-1 (ref. ³⁸; a gift from the Strome laboratory), anti-Flag (F3165, Sigma), anti-GAPDH (Ab125247, Abcam), anti-mCherry (RFP (6G6), Chromotek) and anti-tubulin (Ab6160, Abcam) antibodies, and the secondary antibodies used included anti-rabbit (31460, Pierce), anti-mouse (31430, Pierce) and anti-rat (A9037, Sigma) HRP antibodies. The SuperSignal West Pico PLUS Chemiluminescent Substrate was used to detect the signal using a ChemiDoc MP imaging system (Biorad).

Confocal live imaging. Transgenic worms were mounted on 2% agarose pads in the presence of 0.5% sodium azide. Confocal images were obtained using a ZEISS LSM 700 microscope with a ×40 objective or ×63 objective for the H2B–mCherry quantification. Images were obtained using the ZEISS ZEN microscope software and processed using ImageJ v.2.0.0. The quantification of the histone H2B–mCherry was performed on a single confocal image taken at the surface of the pachytene region of the germline from 12 individual worms. In each worm, the intensity of H2B–mCherry fluorescence was measured in 15 nuclei using ImageJ. The incorporation of histone H2B–mCherry into the chromatin enables the visualization of chromosome compaction. Pachytene nuclei from wild-type and sterile *piwi*-mutant animals were scored for lack of visible signs of chromosome compaction. The scored *piwi*-mutant nuclei were still showing a diffused signal of histone H2B–mCherry in the nucleus. Nuclei with very low histone H2B–mCherry were excluded from counting.

Immunostaining. Plates of adult worms were washed with PBS containing 0.1% Tween (PBST). Ten worms were placed on a polylysine-coated slide in the presence of 0.5% sodium azide, and the gonads of immobilized worms were dissected. The slide was fixed with 1% paraformaldehyde for 5 min, frozen in liquid nitrogen and then immersed for at least 1 min in methanol at –20 °C. The slides were then washed in PBST. Blocking was performed in PBST containing 0.5% BSA. Primary antibodies were diluted in PBST containing 0.5% BSA, and incubated overnight at room temperature. Slides were washed at least three times for 5 min in PBST with 0.5% BSA, and secondary antibodies were added and incubated for 2 h at room temperature. The slides were then washed at least twice in PBST with 0.5% BSA and were then counterstained with DAPI and mounted using Vectashield. The primary antibodies used were anti-Flag (Sigma, F1804) antibodies at a dilution of 1:500, and the secondary antibodies used were goat anti-mouse (Invitrogen, Alexa Fluor 488) antibodies at a dilution of 1:500.

RNA IP. A synchronous population of 40,000 worms was collected 48 h after hatching and suspended in extraction buffer (50 mM HEPES pH 7.5, 300 mM NaCl, 5 mM MgCl₂, 10% glycerol, 0.25% NP-40, protease inhibitor cocktails (Fermentas)), and samples were treated by 30 strokes using a metal dounce on ice. Crude protein extracts were centrifuged at 12,000 r.p.m. at 4 °C for 10 min. Protein concentration was quantified using the Bradford assay, and 1 mg of protein extract was incubated with 15 µl of packed anti-Flag M2 magnetic agarose beads (Sigma, M8823) for 1 h at 4 °C. After four washes with extraction buffer, the IP protein was eluted twice with 100 µl of 3×Flag peptide (Sigma, F4799) for 30 min at 4 °C. The eluate was next incubated with 750 µl of TRI reagent (MRC) to extract the immunoprecipitated RNAs. Then, 750 µl of TRI reagent (MRC) was also added to 10% of protein extract before the IP (input). The extracted RNA was then analysed using RT–qPCR to quantify mRNA or used to clone sRNAs.

RT–qPCR. DNase-treated total RNA (1 µg) was used as a template to generate cDNA, using random hexamer primers and M-MLV reverse transcriptase, and the qPCR reactions were performed using Applied Biosystems Power up SYBR Green PCR Master mix following the manufacturer's instructions and using an Applied Biosystems QuantStudio 3 Real-Time PCR System. The primers used for the qPCR are provided in Supplementary Table 5.

ChIP. ChIP procedures were as described previously⁹ with the following modification. We collected eggs by hypochlorite treatment, and synchronous populations of worms were grown for 48 h after hatching at 20 °C on OP-50 *E. coli* at a density of approximately 40,000 animals per Petri dish (15 cm). Approximately

2 mg of protein chromatin extract was used for each ChIP experiment. The RFP-Trap coupled to agarose beads (Chromotek) was used for IP of chromatin extracts, and was performed for 2 h at 4 °C. The primers used for the qPCR are provided in Supplementary Table 5.

Sequencing data analyses. *RNA-seq.* Multiplexed Illumina sequencing data were demultiplexed using Illumina bcl2fastq converter (v.2.17.1.14). The read quality of all of the libraries was assessed using fastQC (v.0.11.5). Fastq reads were aligned on the *C. elegans* genome (ce11, *C. elegans* Sequencing Consortium WBcel235) using HISAT2 (ref. ⁶³) v.2.0.4 with the default settings. After alignment to the *C. elegans* genome sequence, featureCounts⁶⁴ v.1.5.2 was used to count reads mapped to annotated genomic features, such as protein-coding genes, pseudogenes, RNA transposons, DNA transposons, simple repeats, satellites, rRNAs, transfer RNAs, small nuclear RNAs (snRNAs), small nucleolar RNAs (snoRNAs), antisense RNAs. Annotations were obtained from the Ensembl release 81 as distributed in the Illumina iGenomes collection, with the exception of repetitive sequences, which were obtained from the repeatMasker annotation file present in the UCSC genome annotation database for the February 2013 (WBcel235/ce11) assembly of the *C. elegans* genome. Counted reads for each genomic feature were used for differential-expression analysis using the R/Bioconductor package DESeq2 (ref. ⁶⁵) v.1.20.0. Upregulated and downregulated genes were detected on the basis of the differential expression criteria of adjusted $P < 0.05$ and at least a twofold increase or decrease in expression levels relative to the control samples.

sRNA-seq. Multiplexed Illumina sequencing data were demultiplexed using Illumina bcl2fastq converter (v.2.17.1.14). The read quality of all of the libraries was assessed using fastQC. The 3' adapter was trimmed from raw reads using Cutadapt⁶⁶ v.1.15 using the following parameter: -a TGGAAATTCCTCGGGTGCCAAAGG --discard-untrimmed. 5' and 3' end unique molecular identifiers (UMIs) were used to deduplicate the trimmed reads. Deduplication was performed by first sorting reads by sequence using the option -s in fastq-sort (from fastq-tools v.0.8; <https://github.com/dcjones/fastq-tools/tree/v0.8>) and then using a custom Haskell program that retained the best quality reads at each position among reads of identical sequences. Then, 4-nucleotide UMIs were trimmed at both ends using Cutadapt (options, -u 4 and -u -4). Finally, we selected only deduplicated reads ranging from 18 to 26 nucleotides using bioawk (<https://github.com/lh3/bioawk>). The selected 18–26-nucleotide reads were aligned to the *C. elegans* genome sequence (ce11, *C. elegans* Sequencing Consortium WBcel235) using Bowtie2 (ref. ⁶⁷) v.2.3.4.1 with the following parameters: -L 6 -i S,1,0.8 -N 0. A custom Python script was used to classify reads into sRNA categories on the basis of the known annotations at their mapping positions, their orientation with respect to these annotations, and their length and starting nucleotide. Annotation sources were the same as for RNA-seq analyses. Roughly, reads matching piRNA (allowing for up to 26 nucleotides to account for the possible presence of not completely matured piRNAs) or miRNA annotations were classified as such. 21–23-nucleotide reads that were not classified as piRNAs or miRNAs and that started with G were classified as potential 22G-RNAs and were further classified into sub-categories on the basis of them being antisense to protein-coding genes, pseudogenes, RNA transposons, DNA transposons, simple repeats or satellites. We call the set of all of these antisense 22G-RNAs 'si 22G'. Reads per million (RPM) were calculated by dividing the read counts by the total number of reads minus structural RNAs—that is, sense sRNA reads that were probably derived from degraded rRNAs, tRNAs, snRNAs or snoRNAs, as estimated by running featureCounts on the mapped 18–26-nucleotide reads—and multiplied per 1,000,000. Next, log₂-transformed fold changes were calculated for each replicate, adding 0.25 RPM as a pseudocount, and the mean value across replicates was used. For IP experiments, we calculated the RPM of the reads from input and from IP. Next, we calculated the log₂-transformed fold changes between IP versus input. sRNAs from genes with log₂-transformed fold changes of at least 1 in IP versus input were considered to be associated with the IP AGO protein.

GRO-seq. Multiplexed Illumina sequencing data were demultiplexed using Illumina bcl2fastq converter (v.2.17.1.14). The read quality of all of the libraries was assessed using fastQC. The 3' adapter was trimmed from raw reads using Cutadapt (option, -a TGGAAATTCCTCGGGTGCCAAAGG). Only reads with at least 24 nucleotides after trimming (but including 5' and 3' randomized tetramers) were retained (option -m 24). Reads in which the adapter was not found were also retained (option, --untrimmed-output). 5' and 3' end tetramers were removed using Cutadapt (options -u 4 and -u -4). The reads were aligned on the *C. elegans* genome (ce11, *C. elegans* Sequencing Consortium WBcel235) using Bowtie2 with the default parameters. After alignment to the *C. elegans* genome, read counting using featureCounts and differential expression analysis using DESeq2 were performed as described for the RNA-seq data, using the same criteria to detect upregulated and downregulated genes.

Generation of bigwig files. For all of the library types, normalized bigwig files were generated from the mapping results using millions of non-structural mappers as a normalization factor. This normalized coverage information was computed for 10 bp bins using the bedtools⁶⁸ and bedops⁶⁹ v.2.4.26 packages.

Comparison between RNA-seq or GRO-seq and sRNA-seq. To compare RNA-seq or GRO-seq and sRNA-seq data, plots were generated by plotting, in DESeq2, log₂-transformed fold changes of the RNA-seq (or GRO-seq) data against the RPM fold changes of the si_22G sRNA category using custom Python scripts.

Metaprofile. Metaprofiles were generated using RPM from sRNA-seq analysis by summarizing normalized coverage information (taken from bigwig files and averaged across replicates) along histone genes or 200 nucleotides upstream and downstream of the stem-loop structure of histone mRNAs using the deepTools⁷⁰ package v.3.1.2.

Gene lists. The gene lists used are provided in Supplementary Table 6.

Statistics and reproducibility. Almost all of the experiments shown in this study were performed independently at least twice and no inconsistent results were observed. All attempts at replication were successful. IP and MS experiments were conducted with four biological replicates. All of the RNA-seq experiments were performed using two biological replicates. For details of the particular statistical analyses used, precise *P* values, statistical significance and sample sizes for all of the graphs, see the figure legends and the Methods. The source data for Figs. 1–6 and Extended Data Figs. 1–6 are provided.

Reporting Summary. Further information on research design is available in the Nature Research Reporting Summary linked to this article.

Data availability

All sequencing data (GRO-seq, RNA-seq and sRNA-seq from total lysate or IP experiments) are available at the Gene Expression Omnibus (GEO) under accession code GSE125601. The MS proteomics data have been deposited to the ProteomeXchange Consortium via the PRIDE partner repository with the dataset identifier PXD012557. All other data supporting the findings of this study are available from the corresponding author on reasonable request. Source data are available online for Figs. 1–6 and Extended Data Figs. 1–6.

Code availability

The custom scripts generate for this study are available from the corresponding author on reasonable request.

References

- Brenner, S. The genetics of *Caenorhabditis elegans*. *Genetics* **77**, 71–94 (1974).
- Paix, A., Folkmann, A., Rasoloson, D. & Seydoux, G. High efficiency, homology-directed genome editing in *Caenorhabditis elegans* using CRISPR-Cas9 ribonucleoprotein complexes. *Genetics* **201**, 47–54 (2015).
- Arribere, J. A. et al. Efficient marker-free recovery of custom genetic modifications with CRISPR/Cas9 in *Caenorhabditis elegans*. *Genetics* **198**, 837–846 (2014).
- Aoki, K., Moriguchi, H., Okawa, K. & Tabara, H. Biochemical genetic analyses of RdRP and Slicer activities related to RNAi in *C. elegans*. in *International Worm Meeting* (2007).
- Edgley, M. L., Baillie, D. L., Riddle, D. L. & Rose, A. M. in *WormBook* (The *C. elegans* Research Community, 2006).
- Kamath, R. S. & Ahringer, J. Genome-wide RNAi screening in *Caenorhabditis elegans*. *Methods* **30**, 313–321 (2003).
- Jayaprakash, A. D., Jabado, O., Brown, B. D. & Sachidanandam, R. Identification and remediation of biases in the activity of RNA ligases in small-RNA deep sequencing. *Nucleic Acids Res.* **39**, e141 (2011).
- Cecere, G., Hoersch, S., O'Keeffe, S., Sachidanandam, R. & Grishok, A. Global effects of the CSR-1 RNA interference pathway on the transcriptional landscape. *Nat. Struct. Mol. Biol.* **21**, 358–365 (2014).
- Poulet, P., Carpentier, S. & Barillot, E. myProMS, a web server for management and validation of mass spectrometry-based proteomic data. *Proteomics* **7**, 2553–2556 (2007).
- Valot, B., Langella, O., Nano, E. & Zivy, M. MassChroQ: a versatile tool for mass spectrometry quantification. *Proteomics* **11**, 3572–3577 (2011).
- Cline, M. S. et al. Integration of biological networks and gene expression data using Cytoscape. *Nat. Protoc.* **2**, 2366–2382 (2007).
- Vizcaino, J. A. et al. 2016 update of the PRIDE database and its related tools. *Nucleic Acids Res.* **44**, D447–D456 (2016).
- Claycomb, J. M. et al. The argonaute CSR-1 and its 22G-RNA cofactors are required for holocentric chromosome segregation. *Cell* **139**, 123–134 (2009).
- Kawasaki, I. et al. The PGL family proteins associate with germ granules and function redundantly in *Caenorhabditis elegans* germline development. *Genetics* **167**, 645–661 (2004).
- Kim, D., Langmead, B. & Salzberg, S. L. HISAT: a fast spliced aligner with low memory requirements. *Nat. Methods* **12**, 357–360 (2015).
- Liao, Y., Smyth, G. K. & Shi, W. FeatureCounts: an efficient general purpose program for assigning sequence reads to genomic features. *Bioinformatics* **30**, 923–930 (2014).

65. Love, M. I., Huber, W. & Anders, S. Moderated estimation of fold change and dispersion for RNA-seq data with DESeq2. *Genome Biol.* **15**, 550 (2014).
66. Martin, M. Cutadapt removes adapter sequences from high-throughput sequencing reads. *EMBnet.journal* **17**, 10–12 (2011).
67. Langmead, B. & Salzberg, S. L. Fast gapped-read alignment with Bowtie 2. *Nat. Methods* **9**, 357–359 (2012).
68. Quinlan, A. R. BEDTools: the Swiss-army tool for genome feature analysis. *Curr. Protoc. Bioinform.* **47**, 11.12.1–11.12.34 (2014).
69. Neph, S. et al. BEDOPS: high-performance genomic feature operations. *Bioinformatics* **28**, 1919–1920 (2012).
70. Ramírez, F. et al. deepTools2: a next generation web server for deep-sequencing data analysis. *Nucleic Acids Res.* **44**, W160–W165 (2016).

Acknowledgements

We thank the members of the Cecere laboratory, D. Canzio, N. Iovino, R. Sawarkar and P. Andersen for discussions of the manuscript; the Miska, the Mello, the Kennedy, the Seydoux, the Claycomb, the Strome and the Dumont laboratories for sharing strains and/or antibodies. Some strains were provided by the CGC, funded by NIH Office of Research Infrastructure Programs (P40 OD010440). This project has received funding from the Institut Pasteur, the CNRS and the European Research Council (ERC) under the EU Horizon 2020 research and innovation programme under grant agreement no. ERC-StG- 679243. G.B. is part of the Pasteur–Paris University (PPU) International PhD Program and has received funding from the EU Horizon 2020 research and innovation programme under the Marie Skłodowska-Curie grant agreement no. 665807. E.C. was supported by a Pasteur-Cantarini Fellowship program. F.D. and D.L. have received funding from Région Ile-de-France and Fondation pour la Recherche Médicale grants to support this study.

Author contributions

G.C. identified and developed the core questions addressed in the project and analysed the results of all of the experiments. G.B. performed most of the experiments and helped to analyse the results. E.C. conceived and generated all of the CRISPR–Cas9 lines used in this study, designed and performed the experiment using a catalytic mutant of CSR-1 and performed all of the confocal live-imaging experiments. M.S. performed all of the co-IP and IP experiments for MS and co-IPs. F.D. and D.L. performed the MS and analysed the data together with M.S. and G.C. B.L. performed the bioinformatics analysis of all sequencing data. M.U. performed some RNA extractions and the RT–qPCR experiment. A.S. performed the brood-size analysis of the RNAi experiments under the supervision of G.B. C.D. performed the brood-size analysis of some of the RNAi and crossing experiments together with G.C. P.Q. performed the GRO-seq. E.C. and P.Q. contributed to collecting some of the RNA samples that were used for the initial RNA-seq experiments. G.C. wrote the paper with contributions from G.B., E.C., M.S. and B.L.

Competing interests

The authors declare no competing interests.

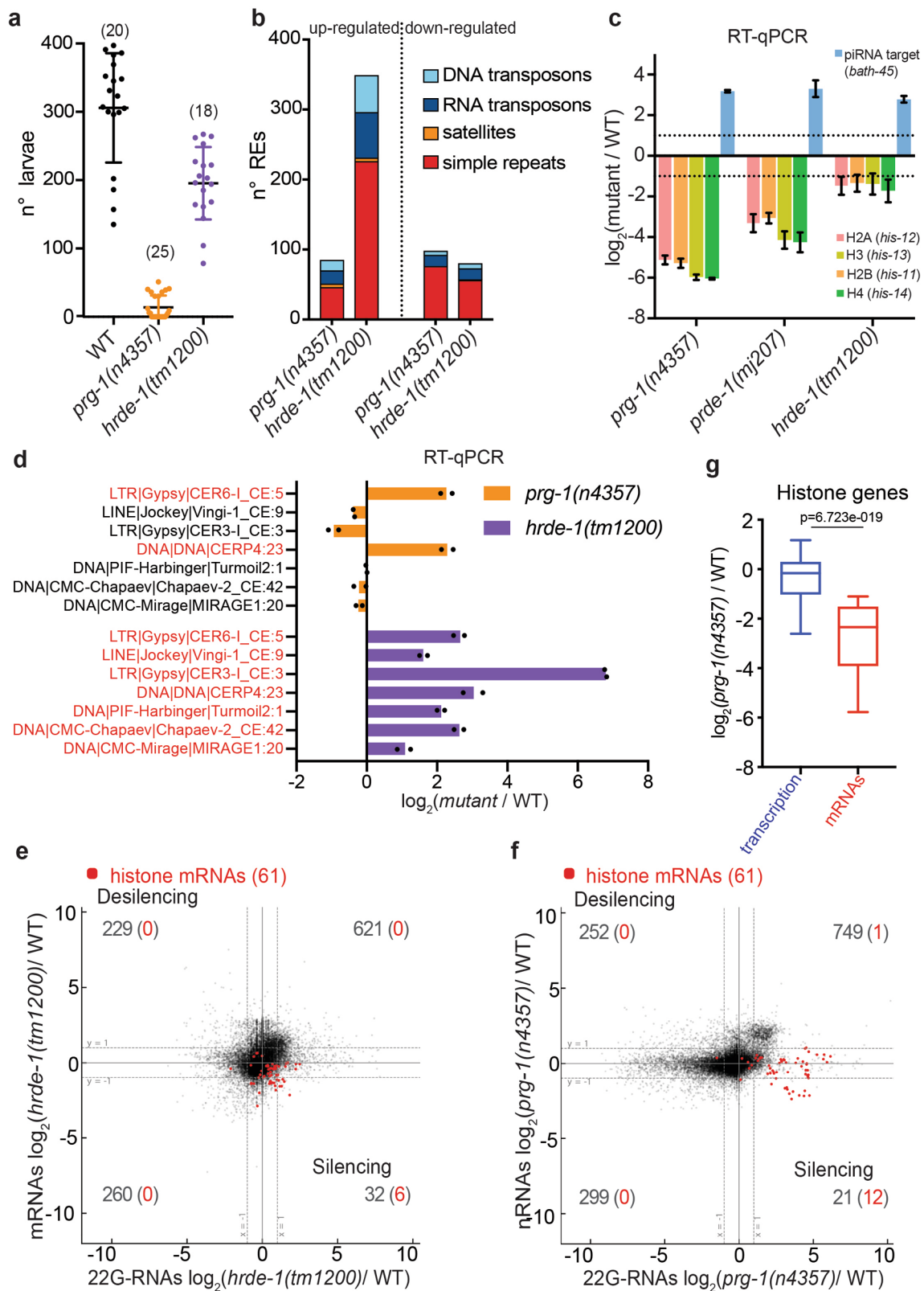
Additional information

Extended data is available for this paper at <https://doi.org/10.1038/s41556-020-0462-7>.

Supplementary information is available for this paper at <https://doi.org/10.1038/s41556-020-0462-7>.

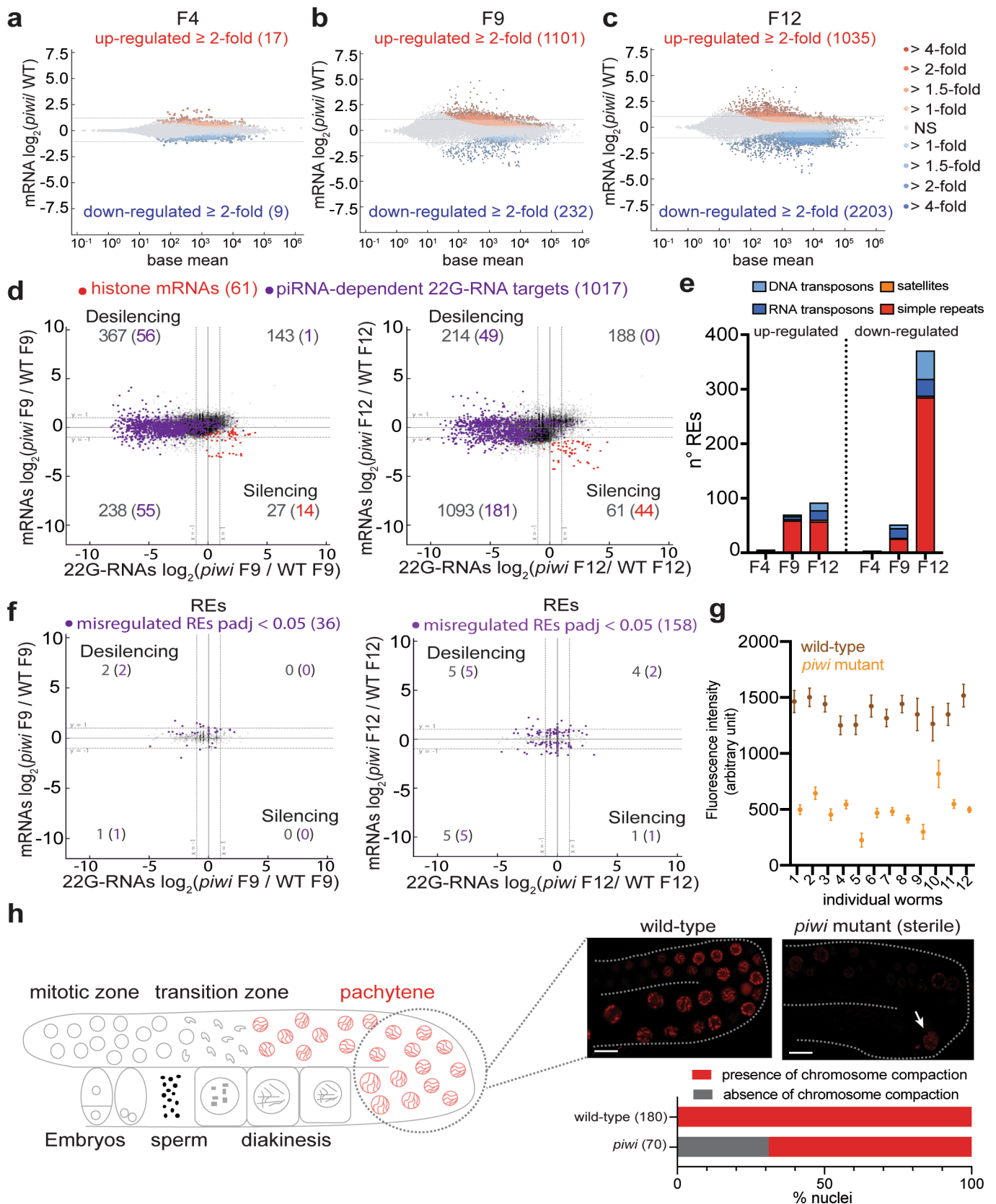
Correspondence and requests for materials should be addressed to G.C.

Reprints and permissions information is available at www.nature.com/reprints.



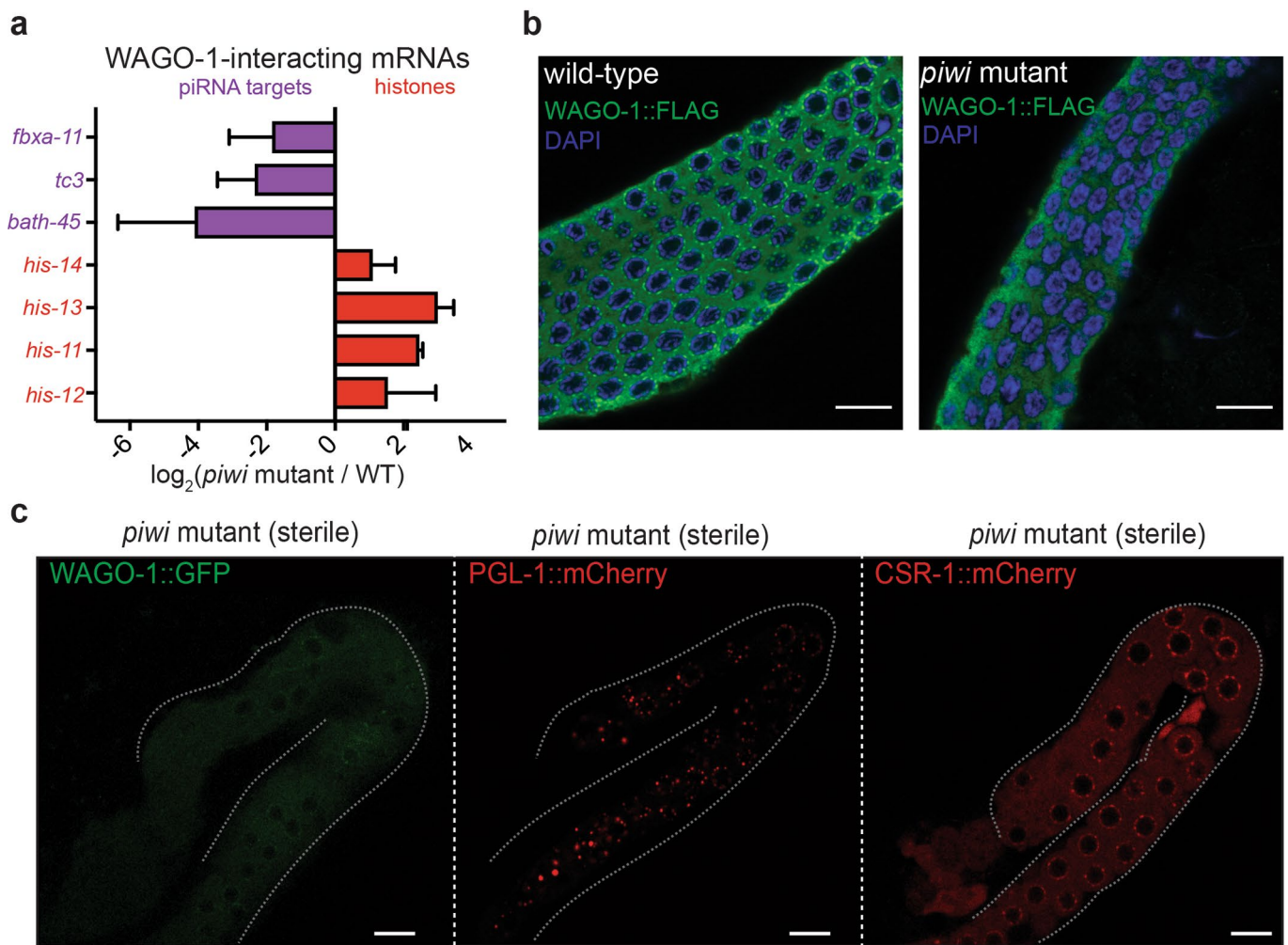
Extended Data Fig. 1 | See next page for caption.

Extended Data Fig. 1 | Histone silencing occurs at the post-transcriptional level only in mutants of the piRNA biogenesis pathway. **a**, Brood size assay of wild-type, *prg-1* (*n4357*) and *hrde-1* (*tm1200*) mutant worms as in Fig. 1d. The black lines indicate the mean, the error bars the standard deviation, and the n (animals) is indicated above in parenthesis. **b**, Number of individual misregulated REs by RNA-seq (≥ 2 -fold and $\text{padj} < 0.05$, Wald test) in *piwi* or *hrde-1* mutants. Data shown represent average of two biologically independent replicates. **c**, RT-qPCR \log_2 fold change of histone mRNAs and piRNA-dependent 22G-RNA targets in *prg-1* (*n4357*), *prde-1* (*mj207*), and *hrde-1* (*tm1200*) mutants compared to wild-type worms. The bars indicate the mean and error bars indicate the standard deviation. $n = 3$ biologically independent experiments. **d**, RT-qPCR showing \log_2 fold change of individual DNA or RNA transposons in mutant vs. wild-type. Up-regulated transposons by RNA-seq are labelled in red. The bars indicate the mean and the black dots individual data from two biologically independent experiments. **e**, mRNA \log_2 fold change (y axis) and 22G-RNA \log_2 fold change (x axis) in *hrde-1*(*tm1200*) mutant vs. wild-type worms for protein-coding genes as in Fig. 1a. Wald test was used to calculate the p value. Data shown represent average of two biologically independent replicates. **f**, nascent RNA (nRNA) \log_2 fold change (y axis) and 22G-RNA \log_2 fold change (x axis) in *prg-1* (*n4357*) mutant vs. wild-type worms for protein-coding genes. Red dots indicate the replicative histone genes. Wald test was used to calculate the p value. Data shown represent average of two biologically independent replicates. **g**, Box plot showing transcriptional (GRO-seq) and post-transcriptional (RNA-seq) histone gene expression changes in *prg-1* (*n4357*) mutant vs. wild-type worms. The median (line), first and third quartiles (box), and whiskers (5th and 95th percentile) are shown. Two-tailed p value calculated with the Mann-Whitney-Wilcoxon tests is shown, using the sample size n (number of genes) = 61. Source data are available in Source Data Extended Data Fig. 1.

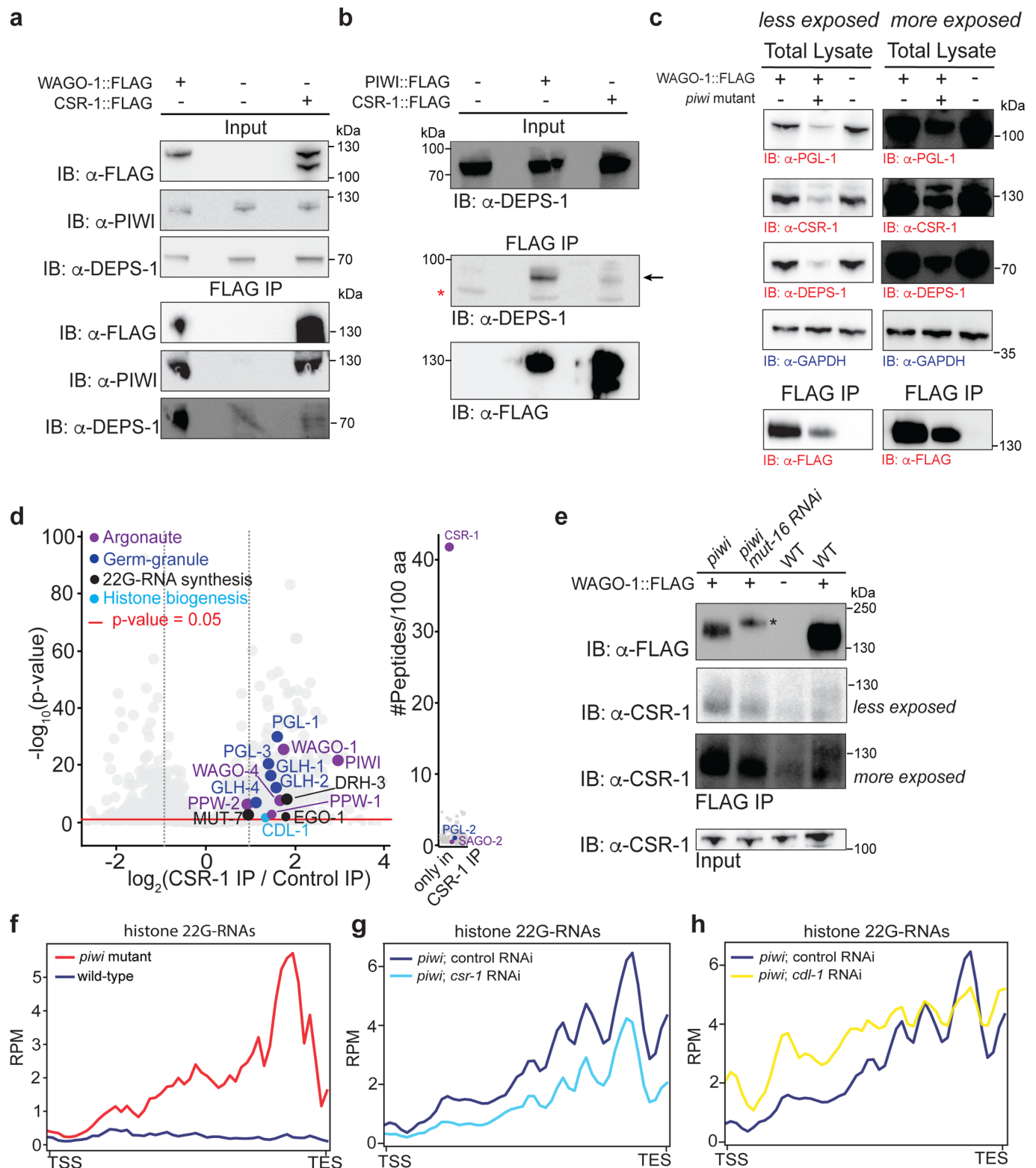


Extended Data Fig. 2 | See next page for caption.

Extended Data Fig. 2 | Transgenerational gene expression changes of protein-coding genes and REs in *piwi* mutant. **a–c**, MA-plot showing mRNA \log_2 fold change between *piwi* mutant and wild-type lines at different generations. Red and blue dots correspond to significant \log_2 fold change ($p_{\text{adj}} < 0.05$, Wald test). The number in parenthesis indicates the number of misregulated genes ≥ 2 -fold. The average from two biologically independent replicates is shown. **d**, Comparison between mRNA \log_2 fold change (y axis) by and 22G-RNA \log_2 fold change (x axis) as shown in Fig. 1a using *piwi* mutant and wild-type CRISPR-Cas9 lines at F9 (left) and F12 (right). **e**, Plot showing the number of individual up-regulated and down-regulated REs by RNA-seq ($p_{\text{adj}} < 0.05$, Wald test) in *piwi* mutant compared to wild-type CRISPR-Cas9 lines at F4, F9, and F12. Only uniquely mapped reads were considered for this analysis. Data shown represent average of two biologically independent replicates. **f**, Comparison between RNA \log_2 fold change (y axis) by and 22G-RNA \log_2 fold change (x axis) as shown in Fig. 1a using *piwi* mutant and wild-type CRISPR-Cas9 lines at F9 (left) and F12 (right). Significant misregulated RE families are indicated ($p_{\text{adj}} < 0.05$, Wald test). The average from two biologically independent replicates is shown. **g**, Average and standard deviation of H2B-mCherry quantification in 15 pachytene nuclei in each individual wild-type and *piwi* mutant worm. $n = 15$ animals. **h**, Visualization of chromosome compaction in pachytene nuclei using H2B-mCherry wild-type and *piwi* mutant worms. The arrow indicates an example of nucleus with defective chromosome compaction in sterile *piwi* mutant. The percentage of nuclei lacking chromosome compaction in *piwi* mutant is shown below the images and the number in parenthesis indicates the number of nuclei counted. The white bars indicate 20 μM size. The experiment was repeated twice with similar results. Statistical source data are available in Source Data Extended Data Fig. 2.

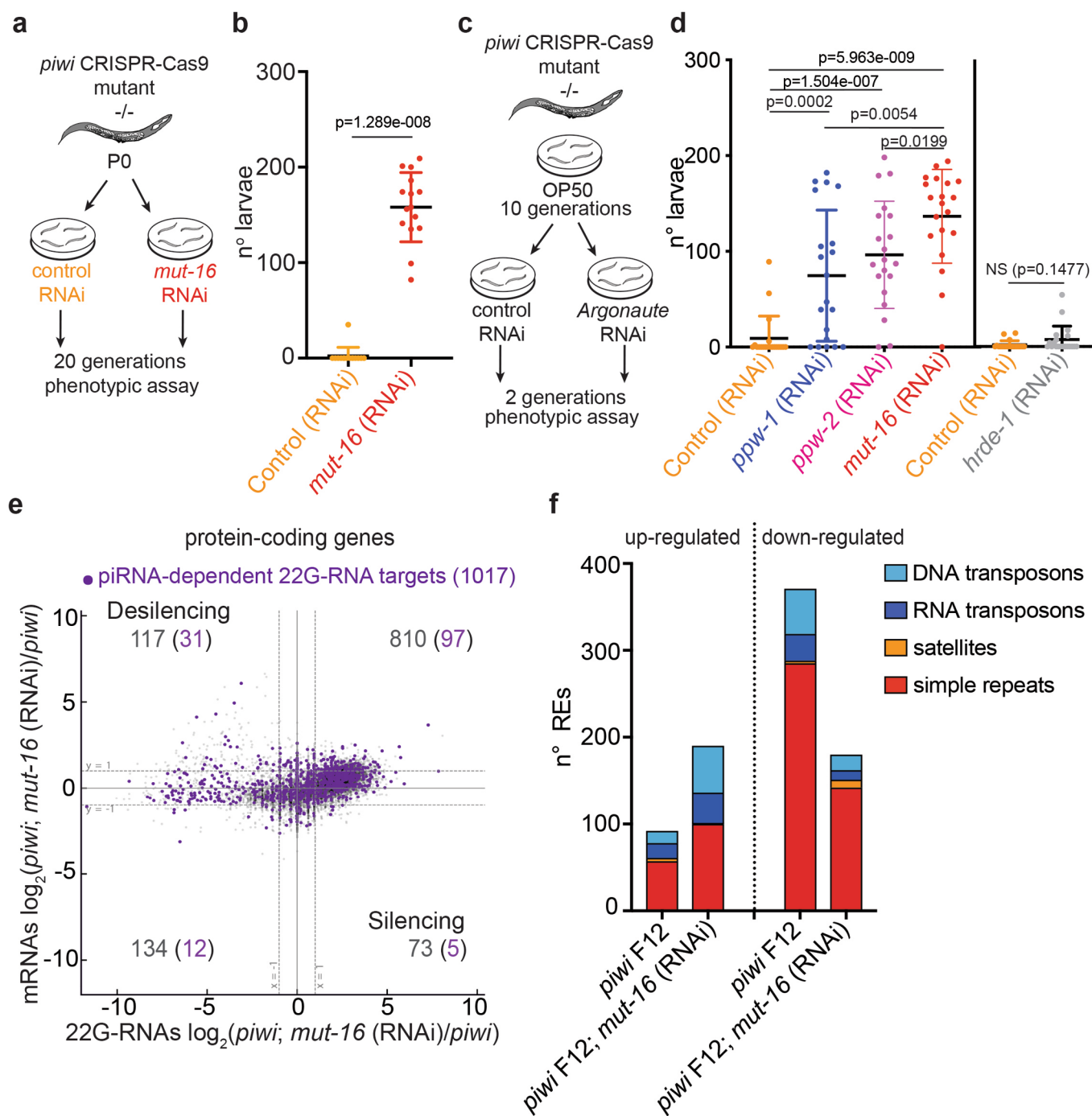


Extended Data Fig. 3 | WAGO-1 relocate from piRNA targets to histone mRNAs. **a**, RNA immunoprecipitation (RIP) experiments followed by RT-qPCR showing the \log_2 fold change of the WAGO-1-interacting mRNAs in *piwi* mutant vs. wild-type worms. The bars indicate the mean and error bars indicate the standard deviation. $n = 4$ biologically independent experiments. **b**, Co-IP experiments showing CSR-1 interactions with WAGO-1 in wild-type and *piwi* mutant worms. Presence (+) or absence (-) of the tagged proteins or *piwi* mutation are indicated. Immunoprecipitation was performed using α -FLAG antibody, and the blots were probed with α -CSR-1 or α -FLAG antibodies. **c**, Immunostaining with α -FLAG antibody showing WAGO-1-FLAG localization in wild-type and *piwi* mutant (green signal). DAPI signal is shown in blue. The white bars indicate 20 μ M size. The experiment was repeated independently twice with similar results. **d**, Live confocal images of WAGO-1-GFP, PGL-1-mCherry, and CSR-1-mCherry in sterile *piwi* mutant germlines. The white bars indicate 10 μ M size. The experiment was repeated independently three times with similar results. Source data are available in Source Data Extended Data Fig. 3.



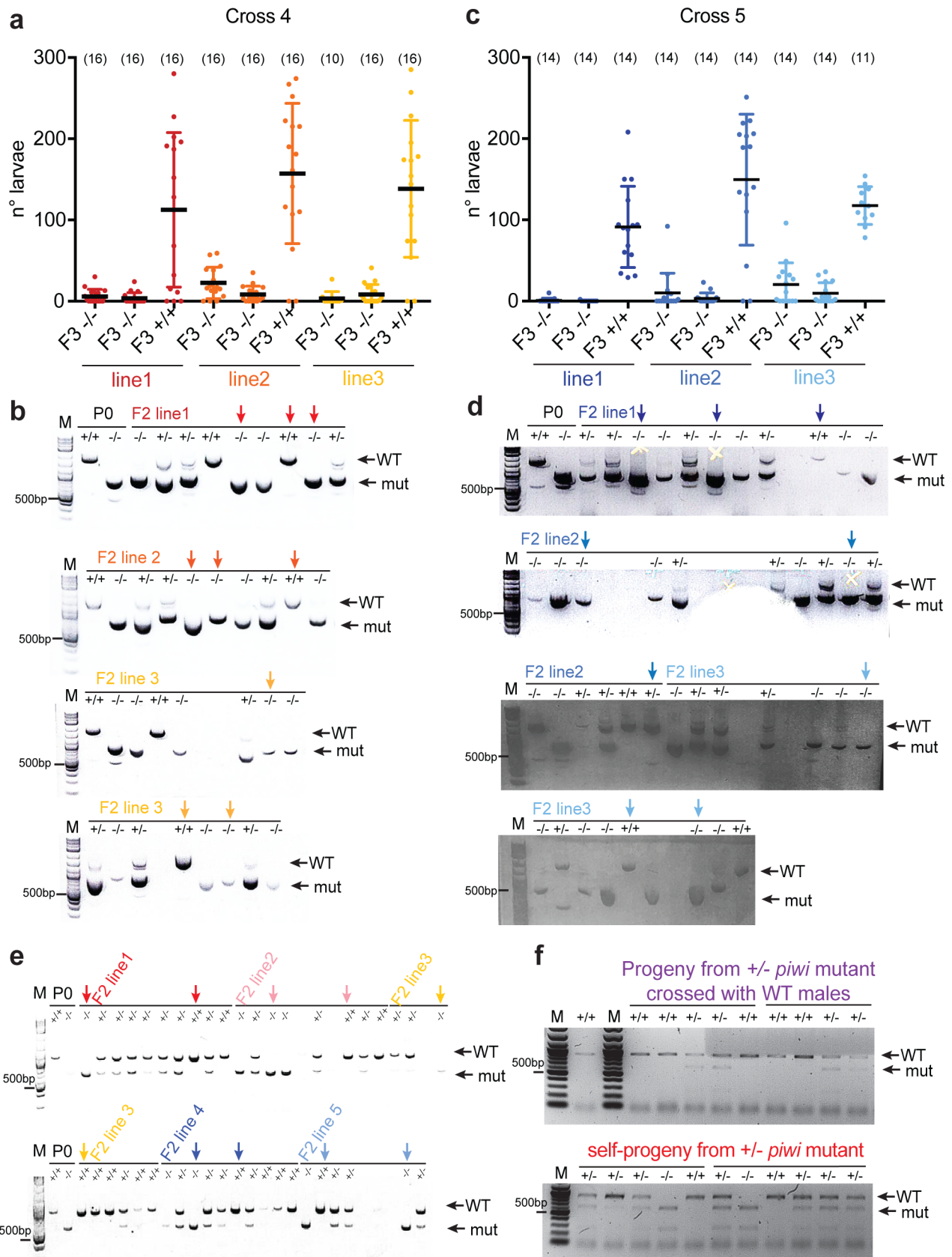
Extended Data Fig. 4 | See next page for caption.

Extended Data Fig. 4 | CSR-1 and CDL-1 contribute to the biogenesis of histone 22G-RNAs in piRNA mutant. **a**, Co-IP experiments using α -FLAG antibody for IPs and α -PIWI, α -DEPS-1 or α -FLAG antibodies for blots. Presence (+) or absence (-) of the FLAG tagged proteins are indicated. The experiment was repeated independently twice with similar results. **b**, Co-IP experiments as in **a**, showing DEPS-1 interaction with PIWI and not with CSR-1. The blots were probed with α -DEPS-1 or α -FLAG antibodies. The experiment was repeated independently twice with similar results. **c**, Immunoblot showing CSR-1, PGL-1, DEPS-1, GAPDH from total protein lysate or FLAG immunoprecipitation in WT and *piwi* mutant worms. Blots for germline-enriched and ubiquitous proteins are shown in red and blue respectively. The experiment was repeated independently twice with similar results. **d**, Volcano plot showing enrichment values and corresponding significance levels for proteins co-purifying with CSR-1 (see also Supplementary Table 1c). Argonaute proteins, germ granule components, 22G-RNA and histone biogenesis factors are indicated. The size of the dots is proportional to the number of peptides used for the quantification. The linear model was used to compute protein quantification ratio and the red horizontal line indicates the two-tailed p value = 0.05. n = 4 biologically independent experiments. **e**, Co-IP experiments as in **a**, showing CSR-1 interaction with WAGO-1 in wild-type, *piwi* mutant and *piwi* mutant treated with *mut-16* RNAi. The blots were probed with α -CSR-1 or α -FLAG antibodies. * The higher migration of this band is due by the GFP fused to WAGO-1-FLAG in this strain. The experiment was repeated independently twice with similar results. **f-h**, Metaprofile analysis showing the distribution of normalized 22G-RNA reads (RPM) across histone genes in wild-type (blue line), *piwi* mutant (red line), and *piwi* mutant animals treated with control RNAi (blue line), *csr-1* RNAi (light blue line) or *cdl-1* RNAi (yellow line). The experiment was repeated independently twice with similar results. Statistical source data and unprocessed blots are available in Source Data Extended Data Fig. 4.



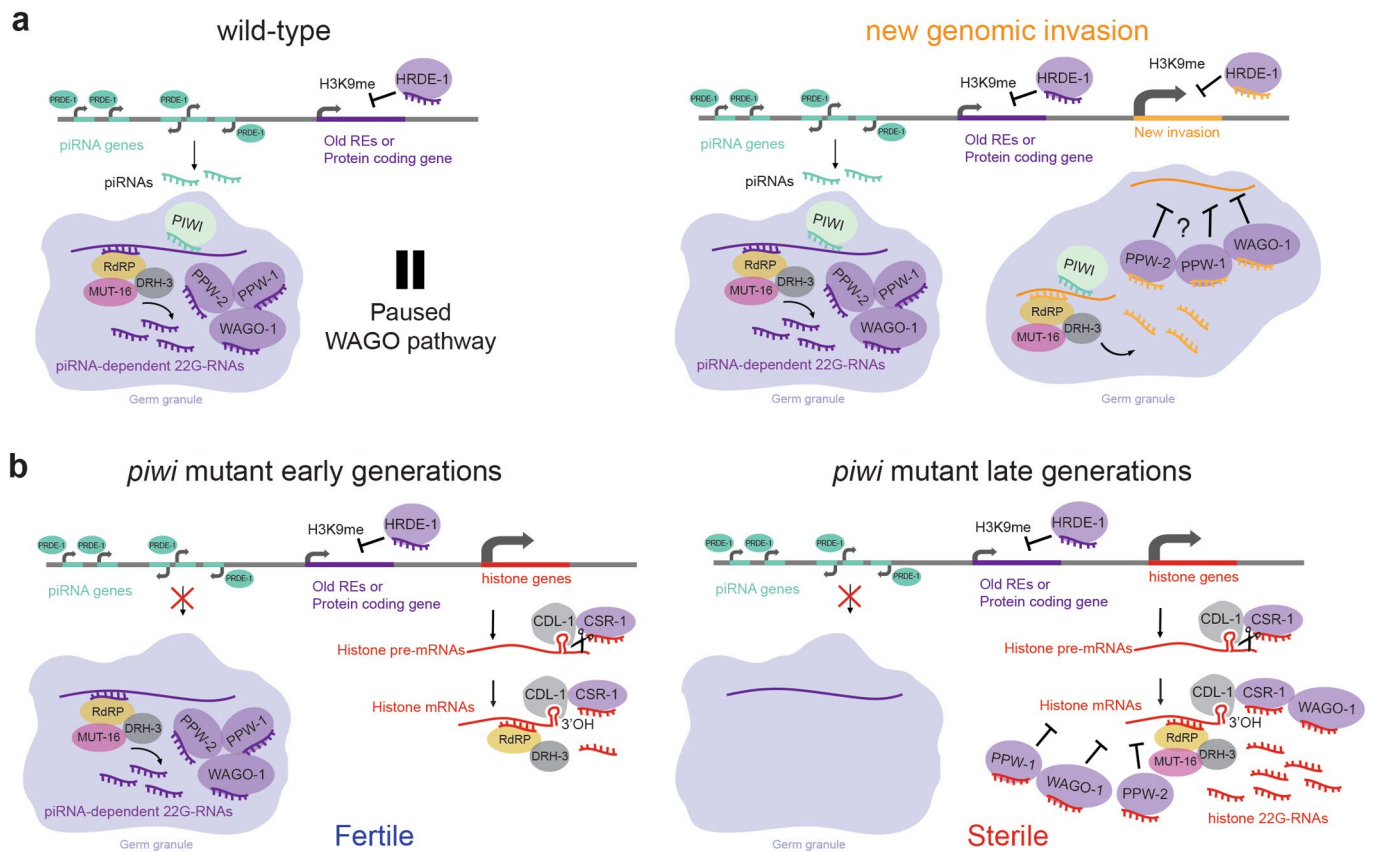
Extended Data Fig. 5 | Depletion of MUT-16, PPW-1, PPW-2 and not HRDE-1 restores fertility in *piwi* mutant independently of REs silencing.

a, Schematic of the RNAi experiment using CRISPR-Cas9 *piwi* mutant worms grown immediately on plates seeded with *E. coli* expressing dsRNA targeting *mut-16* or empty vector for 20 generations. **b**, Results from the experiments described in **a**. Each dot corresponds to the number of alive larvae from individual worms. The black lines indicate the mean and the error bars the standard deviation. Two-tailed p value calculated using the Mann-Whitney-Wilcoxon tests is shown. $n = 15$ animals. **c**, Schematic of the RNAi experiment using CRISPR-Cas9 *piwi* mutant worms grown for 10 generations on plates seeded with *E. coli* OP50 (standard maintenance food) and then shifted for two generations on plates seeded with *E. coli* expressing dsRNA targeting *hrde-1*, *ppw-1*, *ppw-2*, *mut-16* or empty vector. **d**, Results from brood size assay of the experiment described in **c**. The brood size assay is performed as in **b**. *hrde-1* RNAi and its own control has been performed independently from the other RNAi treatment. The black lines indicate the mean and the error bars the standard deviation. Two-tailed p value calculated using the Mann-Whitney-Wilcoxon tests is shown. $n = 20$ animals. **e**, Comparison similar to the one showed in Fig. 1a between mRNA \log_2 fold change (y axis) and 22G-RNA \log_2 fold change (x axis) in *piwi* mutant animals treated with *mut-16* RNAi compared to control RNAi for protein-coding genes. Purple dots indicate the piRNA-dependent 22G-RNA targets. **f**, Plot showing the number of up-regulated and down-regulated individual REs by RNA-seq (padj < 0.05, Wald test) in *piwi* mutant animals treated with control or *mut-16* RNAi. Only uniquely mapped reads were considered for this analysis. Data shown represent average of two biologically independent replicates. Source data available in Source Data Extended Data Fig. 5.



Extended Data Fig. 6 | See next page for caption.

Extended Data Fig. 6 | Decreased fertility in wild-type worms after crossing with piRNA mutants. **a**, Brood size assay similar to the one showed in Fig. 6b of the outcross experiment described in Fig. 6a. One wild-type and two *piwi* mutants were selected from independent F2 heterozygote lines from cross number 4. The black lines indicate the mean, the error bars the standard deviation, and the *n* (animal number analyzed) is indicated in parenthesis. **b**, Genotyping results by electrophoresis gel analysis of the F3 lines derived from self-crossed F2 heterozygote lines. Genomic DNA were extracted from individual animals after they released their progeny and a region spanning *prg-1* mutation was amplified by PCR and digested with a restriction enzyme. The expected mutant and wild-type pattern of digestion is indicated by the black arrows compared to the marker (M). The selected wild-type and *piwi* mutant F3 lines are indicated by arrows with different colors corresponding to the colors used in the brood size assay shown in **a**. The experiment was repeated independently twice with similar results. **c**, same analysis as in **a**, performed with the crossing experiment number 5. The black lines indicate the mean, the error bars the standard deviation, and the sample size (*n*) is indicated in parenthesis. **d**, same analysis as in **b**, performed with the crossing experiment number 5. The experiment was repeated independently twice with similar results. White cross marks in the upper two panels indicate some of the selected lines used) **e**, Genotyping results similar to the one described in **b** using F3 lines derived from the crossing experiment between CRISPR-Cas9 *piwi* mutant hermaphrodite and wild-type males. The experiment was repeated independently twice with similar results. **f**, Genotyping results similar to the one described in **b**. The experiment was repeated independently twice with similar results. Statistical source data are available in Source Data Extended Data Fig. 6.



Extended Data Fig. 7 | Model illustrating the molecular consequences in animals losing piRNAs. a, PRDE-1 promotes the transcription of piRNAs from thousands of genomic loci. piRNAs are then loaded into PIWI, which triggers the biogenesis of WAGO-bound 22G-RNAs from thousands protein-coding genes and REs and keep the WAGO pathway in a paused state (left). In case of new genomic invasions, the piRNAs and WAGOs machineries promptly silence new REs at the transcriptional and the post-transcriptional levels (right). REs can be kept silenced at the chromatin level by H3K9 methyltransferases in a piRNA-dependent or piRNA-independent manner. **b**, In early generations of piRNA mutants (left), the PIWI-induced silencing complex is still maintained on piRNA targets thanks to the interaction with germ granule components. In late generations (right), the piRNA-induced silencing complex is disrupted and some of its components, including WAGO-1, relocalize to the cytoplasm where it interacts with CSR-1 on histone mRNAs to synthesize antisense 22G-RNAs in a CSR-1-dependent manner (right). The PIWI, the WAGO and the CSR-1 pathways share interactions with many RNAi factors and germ granule components in wild-type worms, and in late generations of *piwi* mutants WAGO-1 and possibly PPW-1 and PPW2 become preferentially loaded by CSR-1-dependent histone 22G-RNAs to silence histone mRNAs, which lead to sterility. We propose that the histone mRNA silencing acts as an evolutionary force to maintain a constant production of piRNAs ready to silence new genomic invasion.

Reporting Summary

Nature Research wishes to improve the reproducibility of the work that we publish. This form provides structure for consistency and transparency in reporting. For further information on Nature Research policies, see [Authors & Referees](#) and the [Editorial Policy Checklist](#).

Statistics

For all statistical analyses, confirm that the following items are present in the figure legend, table legend, main text, or Methods section.

n/a Confirmed

- The exact sample size (n) for each experimental group/condition, given as a discrete number and unit of measurement
- A statement on whether measurements were taken from distinct samples or whether the same sample was measured repeatedly
- The statistical test(s) used AND whether they are one- or two-sided
Only common tests should be described solely by name; describe more complex techniques in the Methods section.
- A description of all covariates tested
- A description of any assumptions or corrections, such as tests of normality and adjustment for multiple comparisons
- A full description of the statistical parameters including central tendency (e.g. means) or other basic estimates (e.g. regression coefficient) AND variation (e.g. standard deviation) or associated estimates of uncertainty (e.g. confidence intervals)
- For null hypothesis testing, the test statistic (e.g. F , t , r) with confidence intervals, effect sizes, degrees of freedom and P value noted
Give P values as exact values whenever suitable.
- For Bayesian analysis, information on the choice of priors and Markov chain Monte Carlo settings
- For hierarchical and complex designs, identification of the appropriate level for tests and full reporting of outcomes
- Estimates of effect sizes (e.g. Cohen's d , Pearson's r), indicating how they were calculated

Our web collection on [statistics for biologists](#) contains articles on many of the points above.

Software and code

Policy information about [availability of computer code](#)

Data collection

ChemiDocTM MP imaging system (Biorad) was used to detect chemiluminescent signal from immunoblot membranes.

Applied Biosystems™ QuantStudio™ 3 Real-Time PCR System was used for qPCR

Illumina NextSeq 500 or MiniSeq platforms were used for sequencing

Confocal images were taken using ZEISS LSM 700 microscope with 40X objective or 63X objective for the H2B::mCherry quantification. Images were obtained using ZEISS ZEN black 2.3 SP1.

Data analysis

RNA-seq analysis:

- Demultiplexing with Illumina bcl2fastq converter version v2.17.1.14
- Quality control with fastQC version v0.11.5
-

Alignment with HISAT2 version 2.0.4

- Genomic features annotation with featureCounts version 1.5.2
- Differential gene expression analysis with DESeq2 version 1.20.0

Small RNA-seq and GRO-seq analyses:

- Demultiplexing with Illumina bcl2fastq converter version v2.17.1.14
- Quality control with fastQC version v0.11.5
- 3' adaptor trimming with Cutadapt version 1.15
- Alignment with Bowtie2 version 2.3.4.1
- Metaprofile with deeptools package version 3.1.2

Proteomics:

Caenorhabditis elegans (CAEEL) UP000001940 database using Sequest HF through proteome discoverer (version 2.1) was used to identify C. elegans peptide from mass spectrometry data. The resulting files were further processed using myProMS v3.6. The label free quantification was computed with MassChroQ version 2.2.2. Cytoscape (V 3.7.2) was used to generate the interactome network map. GraphPad Prism Version 8.3.0 and Microsoft Excel Version 16.16.16 were used for statistics.

CRISPR-Cas9:

Unique and specific guide RNA sequences were selected using the off-target prediction CRISPR Design tool at <http://crispr.mit.edu/>. Quantification of confocal images was performed using ImageJ software V2.0.0.

qPCR data were analyzed using QuantStudio™ Design and Analysis software V 2.2

For manuscripts utilizing custom algorithms or software that are central to the research but not yet described in published literature, software must be made available to editors/reviewers. We strongly encourage code deposition in a community repository (e.g. GitHub). See the Nature Research [guidelines for submitting code & software](#) for further information.

Data

Policy information about [availability of data](#)

All manuscripts must include a [data availability statement](#). This statement should provide the following information, where applicable:

- Accession codes, unique identifiers, or web links for publicly available datasets
- A list of figures that have associated raw data
- A description of any restrictions on data availability

All the sequencing data are available at the following accession numbers GSE125601. The mass spectrometry proteomics data have been deposited to the ProteomeXchange Consortium via the PRIDE partner repository with the dataset identifier PXD012557. Source data for Fig. 1,2,3,4,5,6 and Extended Fig. 1,2,3,4,5,6 have been provided. All other data supporting the findings of this study are available from the corresponding author on reasonable request.

Field-specific reporting

Please select the one below that is the best fit for your research. If you are not sure, read the appropriate sections before making your selection.

- Life sciences Behavioural & social sciences Ecological, evolutionary & environmental sciences

For a reference copy of the document with all sections, see [nature.com/documents/nr-reporting-summary-flat.pdf](https://www.nature.com/documents/nr-reporting-summary-flat.pdf)

Life sciences study design

All studies must disclose on these points even when the disclosure is negative.

Sample size	For immunoprecipitation and mass spectrometry or Co-IP synchronous population of 120,000 (for CSR-1, PRG-1 IPs) or 40,000 (for WAGO-1 IPs for mass spectrometry) worms were used at the developmental time point of 48 hours post hatching. Lower number of worms for WAGO-1 IPs was used because of the lower number of piwi mutant worms available. The two sample sizes were experimentally optimized in our laboratory after several tests in collaboration with the mass spectrometry facility. In all the sequencing experiments 40,000 worms were used at the developmental time point of 48 hours post hatching. This sample size has been empirically evaluated to be sufficient to obtain large amount of RNAs, sufficient for multiple applications. For the preparation of total RNA extracted from generation F4 of wild-type and piwi mutant worms 10 manually picked worms were used because we couldn't grow them in large amount at that short generation time. We have optimized our RNA-seq protocol using minimum 10 adult worms after several tests in our laboratory. Sample size for the brood size experiments was determined according to our pre-tests in the lab using at least 10 worms for each strain.
Data exclusions	Dead worms were excluded from the counting in brood size experiments. Nuclei with very low histone H2B::mCherry in piwi mutant were excluded from the counting of chromosome compaction.
Replication	Almost all experiments shown in this study were performed independently at least two times and no inconsistent results were observed. All attempts at replication were successful.
Randomization	In brood size experiments different wild-type and mutant lines were assigned to the researcher using random letters.
Blinding	Investigators were blinded in scoring the brood size of wild-type and mutant worms.

Reporting for specific materials, systems and methods

We require information from authors about some types of materials, experimental systems and methods used in many studies. Here, indicate whether each material, system or method listed is relevant to your study. If you are not sure if a list item applies to your research, read the appropriate section before selecting a response.

Materials & experimental systems

n/a	Involvement
<input type="checkbox"/>	<input checked="" type="checkbox"/> Antibodies
<input checked="" type="checkbox"/>	<input type="checkbox"/> Eukaryotic cell lines
<input checked="" type="checkbox"/>	<input type="checkbox"/> Palaeontology
<input type="checkbox"/>	<input checked="" type="checkbox"/> Animals and other organisms
<input checked="" type="checkbox"/>	<input type="checkbox"/> Human research participants
<input checked="" type="checkbox"/>	<input type="checkbox"/> Clinical data

Methods

n/a	Involvement
<input checked="" type="checkbox"/>	<input type="checkbox"/> ChIP-seq
<input checked="" type="checkbox"/>	<input type="checkbox"/> Flow cytometry
<input checked="" type="checkbox"/>	<input type="checkbox"/> MRI-based neuroimaging

Antibodies

Antibodies used

The antibody used were:
 α -PRG-1 antibody, a gift from the Craig Mello lab, dilution used 1:1000
 α -CSR-1 antibody, a gift from the Claycomb lab, dilution used 1:3000
 α -PGL-1 antibody, a gift from the Strome Lab, dilution used 1:1000
 α -DEPS-1 antibody, a gift from the Strome Lab, dilution used 1:2000
 α -FLAG (F3165, Sigma); dilution used 1:5000
 α -GAPDH (Ab125247, Abcam), dilution used 1:2000
 α -mCherry (RFP antibody [6G6], Chromotek), dilution used 1:2000
 α -tubulin (Ab6160, Abcam), dilution used 1:2000

Validation

α -PRG-1 antibody was validated in Batista, P. J. et al. Mol. Cell (2008). doi:10.1016/j.molcel.2008.06.002;
 α -CSR-1 antibody was validated in Claycomb, J. M. et al. Cell (2009). doi:10.1016/j.cell.2009.09.014.
 α -PGL-1 antibody was validated in Kawasaki, I. et al. Genetics (2004). doi:10.1534/genetics.103.023093
 α -DEPS-1 antibody was validated in Spike, C. A., et al. Development (2008). doi:10.1242/dev.015552
 α -GAPDH (Ab125247, Abcam) has been proven and validated on manufacturer website tested for Western Blot.
 α -mCherry (RFP antibody [6G6], Chromotek) has been proven and validated on manufacturer website tested for Western Blot.
 α -tubulin (Ab6160, Abcam) has been proven and validated on manufacturer website tested for Western Blot.
 α -FLAG (F3165, Sigma) has been proven and validated on manufacturer website tested for Western Blot.

Animals and other organisms

Policy information about [studies involving animals](#); [ARRIVE guidelines](#) recommended for reporting animal research

Laboratory animals

All the data collected for this study derived from hermaphrodite *Caenorhabditis elegans* nematode culture at the developmental time point of 48 hours post hatching.

Wild animals

No wild animals has been used in this study

Field-collected samples

This study did not involve samples collected from the field.

Ethics oversight

No ethical approval was required.

Note that full information on the approval of the study protocol must also be provided in the manuscript.